Published in final edited form as:

*Cell Rep*. 2022 May 31; 39(9): 110888. doi:10.1016/j.celrep.2022.110888.

# *Caulobacter* lipid A is conditionally dispensable in the absence of *fur* and in the presence of anionic sphingolipids

**Justin J. Zik**[1,12], **Sung Hwan Yoon**[2,13], **Ziqiang Guan**[3], **Gabriele Stankeviciute Skidmore**[4,11], **Ridhi R. Gudoor**[5,6], **Karen M. Davies**[5,6,14], **Adam M. Deutschbauer**[7], **David R. Goodlett**[2,8,9], **Eric A. Klein**[4,10,11], **Kathleen R. Ryan**[1,7,15,*]

[1]Department of Plant & Microbial Biology, University of California, Berkeley, Berkeley, CA 94720, USA

[2]Department of Microbial Pathogenesis, University of Maryland School of Dentistry, Baltimore, MD 21201, USA

[3]Department of Biochemistry, Duke University Medical Center, Durham, NC 27710, USA

[4]Center for Computational and Integrative Biology, Rutgers University-Camden, Camden, NJ 08102, USA

[5]Molecular Biosciences and Integrated Bioimaging Division, Lawrence Berkeley National Laboratory, Berkeley, CA 94720, USA

[6]Department of Molecular and Cell Biology, University of California, Berkeley, Berkeley, CA 94720, USA

[7]Environmental Genomics & Systems Biology Division, Lawrence Berkeley National Laboratory, Berkeley, CA 94720, USA

[8]Department of Biochemistry & Microbiology, University of Victoria, Victoria, BC V8W 2Y2, Canada

[9]University of Victoria-Genome BC Proteomics Centre, Victoria, BC V8Z 7X8, Canada

[10]Biology Department, Rutgers University-Camden, Camden, NJ 08102, USA

[11]Rutgers Center for Lipid Research, Rutgers University, New Brunswick, NJ 08901, USA



*Correspondence: krr@berkeley.edu.

AUTHOR CONTRIBUTIONS

J.J.Z., E.A.K., and K.R.R. conceived the project. Mass spectrometry experiments were performed and analyzed by S.H.Y., D.R.G., and Z.G. Electron cryotomography experiments were performed and analyzed by R.R.G. and K.M.D. RB-TnSeq experiments, sequencing, and data analysis were performed by J.J.Z., A.M.D., and K.R.R. All other experiments were performed and analyzed by J.J.Z., G.S.S., E.A.K., and K.R.R. The manuscript was written by J.J.Z., E.A.K., and K.R.R. with input from all authors.

DECLARATION OF INTERESTS

J.J.Z. and K.R.R. have applied for US (62/914,271) and international (PCT/US20/28,464) patents on lipid A-deficient *Caulobacter*.

SUPPLEMENTAL INFORMATION

Supplemental information can be found online at https://doi.org/10.1016/j.celrep.2022.110888.

SUPPORTING CITATIONS

The following references appear in the supplemental information: Altschul, 1997; Altschul et al., 1990; Blondelet-Rouault et al., 1997; Skerker et al., 2005.

[12]Present address: Infectious Diseases Translational Research Programme, Department of Microbiology and Immunology, Yong Loo Lin School of Medicine, National University of Singapore, Singapore 117545, Singapore

[13]Present address: National Institute of Allergy and Infectious Diseases, Bethesda, MD 20892-0421, USA

[14]Present address: Diamond Light Source Ltd., Harwell Science & Innovation Campus, Didcot, Oxfordshire OX11 0DE, UK

[15]Lead contact

## SUMMARY

Lipid A, the membrane-anchored portion of lipopolysaccharide (LPS), is an essential component of the outer membrane (OM) of nearly all Gram-negative bacteria. Here we identify regulatory and structural factors that together render lipid A nonessential in *Caulobacter crescentus*. Mutations in the ferric uptake regulator *fur* allow *Caulobacter* to survive in the absence of either LpxC, which catalyzes an early step of lipid A synthesis, or CtpA, a tyrosine phosphatase homolog we find is needed for wild-type lipid A structure and abundance. Alterations in Fur-regulated processes, rather than iron status per se, underlie the ability to survive when lipid A synthesis is blocked. Fitness of lipid A-deficient *Caulobacter* requires an anionic sphingolipid, ceramide phosphoglycerate (CPG), which also mediates sensitivity to the antibiotic colistin. Our results demonstrate that, in an altered regulatory landscape, anionic sphingolipids can support the integrity of a lipid A-deficient OM.

## Graphical Abstract

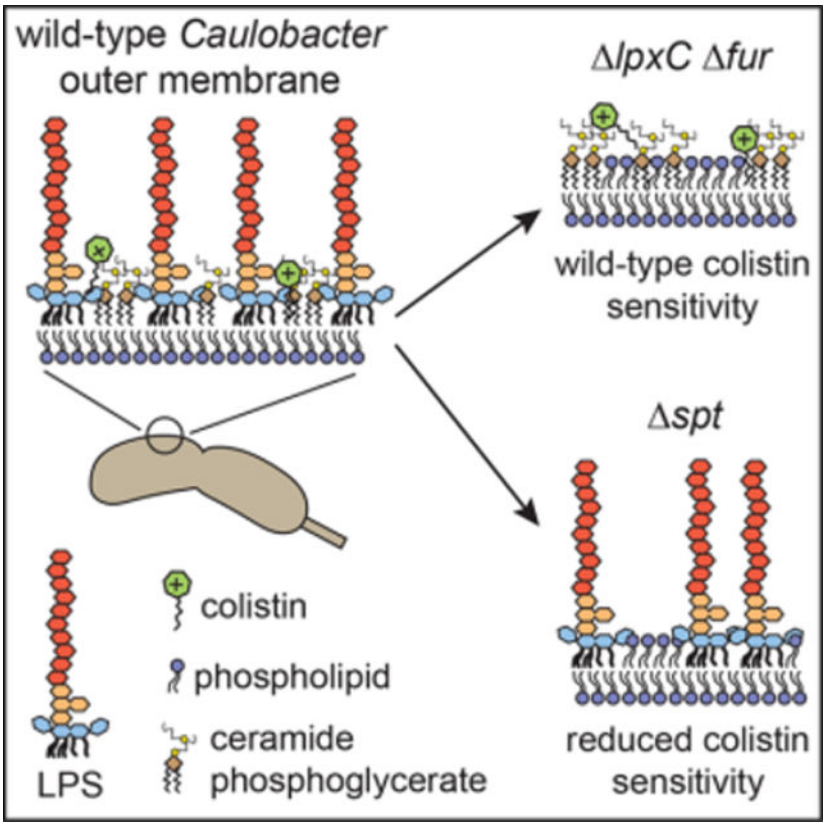


## In brief

Lipid A, the membrane-anchoring segment of lipopolysaccharide, is generally considered to be an essential component of the Gram-negative bacterial outer membrane. Zik et al. show that deletion of the transcriptional regulator *fur* and synthesis of the anionic sphingolipid ceramide phosphoglycerate enable *Caulobacter crescentus* to survive without lipid A.

## INTRODUCTION

Gram-negative bacteria are enclosed in a three-layer envelope composed of the inner membrane (IM) or cytoplasmic membrane, a thin layer of peptidoglycan (PG), and an outer membrane (OM). The OM is an asymmetric bilayer, with phospholipids populating the inner leaflet and lipopolysaccharide (LPS) predominating in the outer leaflet. The canonical LPS structure of *Escherichia coli* comprises three segments: (1) lipid A, a hexa-acylated, phosphorylated glucosamine disaccharide anchored in the membrane; (2) a core oligosaccharide usually shared by members of the same species; and (3) a repeating polysaccharide (O-antigen) that can vary highly among strains of the same species (Whitfield and Trent, 2014). LPS confers robust barrier function upon the OM, making it inherently less permeable than the IM to small hydrophobic compounds (Nikaido, 2003).

Although the O-antigen and core oligosaccharide are nearly always dispensable, it is widely accepted that lipid A is essential for viability of Gram-negative bacteria. Some exceptions to this rule are species that possess a dual membrane system but naturally lack lipid

A, such as *Sphingomonas* spp. and the spirochetes *Borrelia burgdorferi* and *Treponema pallidum* (Kawahara et al., 1991; Kawasaki et al., 1994; Radolf and Kumar, 2018). Efforts to eliminate lipid A from *E. coli* strains have found that the intermediate molecule lipid $IV_A$ is sufficient for viability only when the strain has compensatory mutations that promote export of this species across the IM (Mamat et al., 2008; Meredith et al., 2006). To date, lipid A-deficient mutants have been recovered in *Neisseria meningitidis, Moraxella catarrhalis,* and *Acinetobacter baumannii* (Moffatt et al., 2010; Peng et al., 2005; Steeghs et al., 1998). It remains unclear why at least a minimal lipid A structure is essential in some Gram-negative bacteria but not others.

Lipid A is synthesized by the highly conserved Raetz pathway (Whitfield and Trent, 2014), but significant variation exists in lipid A structures. In many species, the 1- and 4′-phosphates of lipid A can be modified to decrease negative charge and reduce susceptibility to cationic antimicrobial peptides (CAMPs; Moffatt et al., 2019). In a few species, replacement of the 1- and/or 4′-phosphates of lipid A with sugars is constitutive (De Castro et al., 2008; Plötz et al., 2000). The predominant lipid A species in the alphaproteobacterium *Caulobacter crescentus* (Smit et al., 2008) varies from that of *E. coli* (Qureshi et al., 1988) in that the central glucosamine disaccharide is replaced by two 2,3-diamino-2,3-dideoxy-D-glucopyranose (GlcN3N) residues, and the 1- and 4′-phosphates are replaced by galactopyranuronic acid (Gal*p*A) residues.

The tyrosine phosphatase homolog *ctpA* is essential for viability and is implicated in cell envelope maintenance, but its molecular function is unknown (Shapland et al., 2011). Depletion of *ctpA* causes extensive OM blebbing, failure to resolve PG at the division site, and cell death. Here we show that *ctpA* is required for the wild-type structure and abundance of lipid A. A screen for suppressors of *ctpA* essentiality recovered strains with null mutations in the O-antigen biosynthetic pathway or in the ferric uptake regulator *fur*. Surprisingly, mutations in *fur* also permit deletion of *lpxC*, which encodes an otherwise essential enzyme in lipid A synthesis (Whitfield and Trent, 2014). Δ*ctpA* and Δ*lpxC* strains containing suppressor mutations have significantly reduced or undetectable levels of lipid A, respectively.

To uncover mechanisms that promote survival in the absence of lipid A, we used random barcode-transposon site sequencing (RB-TnSeq). We found that several genes required for sphingolipid synthesis in *Caulobacter* (Stankeviciute et al., 2019, 2022) are important for fitness when lipid A synthesis is chemically inhibited. Because *Sphingomonas* spp. naturally lack LPS and bear anionic sphingolipids on the cell surface (Kawasaki et al., 1994), we hypothesized that anionic sphingolipids could support viability in the *Caulobacter* Δ*lpxC* mutant. Indeed, we identified a sphingolipid species, ceramide phosphoglycerate, that is produced in wild-type cells and is a critical fitness factor in the absence of lipid A. We also found that ceramide phosphoglycerate, rather than LPS, underlies *Caulobacter*'s sensitivity to the CAMP colistin.

## RESULTS

### Suppressor mutations affecting Fur or O-antigen synthesis permit loss of *ctpA*

We used a CtpA depletion strain from a prior study to identify mutations that would support *Caulobacter* viability in the absence of CtpA (Shapland et al., 2011). Regulated depletion of CtpA in KR3906 is achieved by expressing *ctpA*::*3x-FLAG*::*ssrA* from a xylose-inducible promoter (Meisenzahl et al., 1997) on a high-copy plasmid in a Δ*ctpA* strain also lacking *sspB*. The native CtpA protein could not be depleted without an ssrA tag to target it for proteolysis. However, addition of this tag made CtpA proteolysis so rapid that xylose-dependent expression of CtpA-33FLAG-ssrA did not support viability. Further deleting *sspB*, which encodes a proteolytic adaptor for ssrA-tagged substrates (Levchenko et al., 2000), reduced the basal rate of CtpA-33FLAG-ssrA degradation enough to permit complementation in xylose-supplemented PYE medium (PYEX).

When CtpA is depleted during growth on dextrose-supplemented PYE medium (PYED), KR3906 exhibits division defects, OM blebbing, and death (Figure 1). We UV-mutagenized KR3906, selected strains that grew on PYED, and screened for isolates that were cured of the *ctpA* covering plasmid (Figure 1A). Genome resequencing of 17 confirmed suppressor strains yielded 15 strains with mutations in 9 genes predicted to participate in O-antigen biosynthesis; one strain with a single mutation in *fur*, encoding the ferric uptake regulator; and one strain harboring a mutation in *fur* along with a mutation in an O-antigen biosynthetic gene (Table S1). Although some strains contained point mutations in other genes, every suppressor strain harbored a mutation predicted to affect either O-antigen synthesis or Fur. Because of the frequent occurrence of frameshift or nonsense mutations, we assumed that each mutation disrupted the function of the affected gene.

We chose for further analysis candidate suppressor genes whose functions were well established in *Caulobacter* or other bacteria. *CCNA_00497* encodes a glycosyltransferase necessary for wild-type levels of smooth LPS containing the O-antigen (S-LPS) (Hershey et al., 2019). *CCNA_01553* encodes a glycosyltransferase that initiates O-antigen synthesis on undecaprenyl-phosphate (Toh and Brun, 2008). *CCNA_03733* encodes a homolog of *manC* involved in synthesizing the activated sugar guanosine diphosphate (GDP)-D-mannose (Samuel and Reeves, 2003), which is incorporated into the core oligosaccharide and O-antigen of *Caulobacter* S-LPS (Jones et al., 2015). *CCNA_00055* encodes the iron-responsive transcriptional regulator Fur (da Silva Neto et al., 2009) and is predicted to be functionally distinct among the genes harboring suppressor mutations. We deleted each gene in the wild-type background (NA1000) or in combination with Δ*sspB*, but we were unable to subsequently delete *ctpA* in these strains by double homologous recombination. Therefore, we individually deleted these genes in the depletion strain KR3906 while propagating the strains on PYEX to supply CtpA.

To determine how each deletion affects cells during acute CtpA depletion, we transferred each mutant to PYED and observed cell morphology and viability (Figure 1). Compared with CtpA depletion in KR3906, depletion of CtpA in the Δ*fur* mutant caused much less OM blebbing but still yielded elongated cells indicative of a division defect (Figure 1C). Neither OM blebbing nor cell chaining/elongation was markedly improved when CtpA was

depleted from the strains lacking *CCNA_00497, CCNA_01553*, or *CCNA_03733*. Despite the persistence of morphological defects, deletion of *fur, CCNA_01553,* or *CCNA_03733* significantly improved cell viability during CtpA depletion (Figure 1B). Deletion of *CCNA_00497* improved survival on PYED to a lesser extent despite the fact that two independent strains with point mutations in *CCNA_00497* were isolated in the suppressor screen. Notably, each strain with a mutation in *CCNA_00497* also harbored 1–2 other mutations (Table S1), which may have augmented the fitness of the original isolates.

We acquired stable Δ*ctpA* mutants by passaging each modified CtpA depletion strain (above) in PYED and screening isolates for loss of the *ctpA*-bearing plasmid. The OM of each Δ*ctpA* strain was smooth with minimal blebbing, but chains of cells were still prevalent in the Δ*ctpA* Δ*sspB* Δ*CCNA_01553*, and Δ*ctpA* Δ*sspB* Δ*fur* mutants (Figure 1D). These reconstituted suppressor strains were morphologically similar to the original isolates containing point mutations in the same genes (Figure S1A). Suppressed Δ*ctpA* mutants grew more slowly than the wild-type strain NA1000 and the corresponding *ctpA*$^{+}$ strains, but all achieved similar stationary-phase densities (Figure S1B). As expected, restoring the expression of *fur*, *CCNA_00497*, or *CCNA_03733* using a xylose-inducible promoter reduced the viability of the corresponding Δ*ctpA* mutants (Figure S1C). Thus, null mutations affecting *fur* or O-antigen biosynthesis allow *Caulobacter* to survive without *ctpA*.

It was puzzling that we could not obtain the strains Δ*ctpA* Δ*CCNA_00497*, Δ*ctpA* Δ*CCNA_1553*, Δ*ctpA* Δ*CCNA_03733*, or Δ*ctpA* Δ*fur* (with or without Δ*sspB*) by double homologous recombination, but they were accessible by depleting CtpA and curing the *ctpA* plasmid. A key difference between these two procedures is that double homologous recombination relies on *sacB* counterselection, where the desired mutants must survive on medium containing 3% sucrose. Unlike the Δ*fur* Δ*sspB* parent, Δ*ctpA* Δ*fur* Δ*sspB* cells displayed a growth defect on PYE/3% sucrose (Figure S1D), indicating that Δ*ctpA* confers susceptibility to sucrose, which likely accounts for the discrepancy between the two genetic methods.

To confirm the functions of *CCNA_00497*, Δ*CCNA_01553*, and *CCNA_03733* in O-antigen synthesis, we deleted individual genes in a Δ*sspB* mutant. Cell lysates treated with Proteinase K were probed with antibodies recognizing S-LPS (Figure S2A) or stained with Pro-Q Emerald 300 to detect carbohydrates (Figure S2B). As observed previously, strains lacking *CCNA_01068* (*wbqA*) or *CCNA_01553* lacked S-LPS, whereas S-LPS abundance was reduced in Δ*CCNA_000497* (Walker et al., 1994; Awram and Smit, 2001; Hershey et al., 2019). Deletion of *CCNA_03733* (*manC*) eliminated S-LPS and reduced the size of a species that we propose to be lipid A + core oligosaccharide (Figures S2B–S2C, **). The core oligosaccharide of *Caulobacter* LPS contains a single penultimate mannose residue (Jones et al., 2015); thus, the reduced size of the indicated band for Δ*CCNA_03733* (Figures S2B and S2C, *) may arise from an incomplete core oligosaccharide. S-LPS was restored to each mutant by xylose-driven complementation of the respective genes (Figure S2C). In contrast to strains with mutations in *CCNA_00497*, *CCNA_01553*, or *CCNA_03733*, the Δ*fur* Δ*sspB* mutant contained wild-type levels of S-LPS (Figures S2A and S2B), indicating that *fur* mutations do not suppress the lethality of Δ*ctpA* by eliminating the O-antigen.

### Δ*ctpA and* Δ*lpxC* strains with suppressor mutations contain little or no lipid A

*ctpA* is transcribed divergently from an operon containing the essential genes *msbA*, *lpxJ*, *kdtA*, and *lpxK* (Christen et al., 2011; Zhou et al., 2015), which, in other bacteria, participate in synthesis and export of lipid A + core (Whitfield and Trent, 2014). Because CtpA depletion results in OM defects, and suppressor mutations were identified in O-antigen biosynthetic genes, we hypothesized that *ctpA* is required for some aspect of LPS synthesis or export.

We performed hot aqueous phenol extraction of LPS from suppressor mutants lacking *ctpA*, along with their $ctpA^+$ counterparts, and analyzed them by PAGE and Pro-Q Emerald 300 staining. Full-length S-LPS was recovered from NA1000, Δ*sspB*, and Δ*fur* Δ*sspB* (Figure 2B, ***) but was absent from Δ*sspB* strains lacking *CCNA_00497*, *CCNA_01553*, or *CCNA_03733*. Interestingly, all Δ*ctpA* strains were deficient in low-molecular-weight species that could represent lipid A +/− core (Figure 2B, *, **). We therefore used the *Limulus* amebocyte lysate (LAL) assay to measure lipid A abundance in live *Caulobacter* strains. All Δ*ctpA* mutants contained ~1,000-fold less lipid A than strains encoding this gene (Figure 2A).

Because Δ*ctpA* suppressor mutants survived with drastically reduced amounts of lipid A, we wanted to determine whether mutations in *fur* or O-antigen synthesis could render lipid A completely dispensable. LpxC catalyzes the first committed step in lipid A synthesis, removal of the 2-acetyl group from acylated UDP-GlcNAc (Whitfield and Trent, 2014). The *lpxC* homolog *CCNA_02064* is essential for viability in wild-type *Caulobacter* (Christen et al., 2011). We constructed an LpxC depletion strain (KR4007) analogous to the CtpA depletion strain. We subsequently deleted *fur*, *CCNA_00497*, *CCNA_01553*, or *CCNA_03733* in this strain and examined the effects of acute LpxC depletion. When these genes were intact, LpxC depletion yielded chains of cells with extensive membrane blebs. Mutants lacking a gene for O-antigen synthesis still showed OM blebs and chaining when LpxC was depleted (Figure 3A). The Δ*fur* mutant had far fewer OM blebs upon LpxC depletion, but cells were still frequently elongated or chained (Figure 3A). These morphologies are generally similar to those seen during CtpA depletion, but unlike CtpA, only Δ*fur* allowed significant growth of the LpxC depletion strain on solid PYED medium (Figure 3B).

When we attempted to isolate stable Δ*lpxC* mutants by depleting LpxC and curing the covering plasmid, only the strain harboring a Δ*fur* mutation permitted complete loss of *lpxC* (KR4103). Importantly, we recovered two stable Δ*lpxC* isolates (KR4224 and 4225) from an LpxC depletion strain harboring only Δ*CCNA_00497* and not Δ*sspB* (KR4223), but genome resequencing revealed that they had acquired additional point mutations in *fur* (Table S2). These results demonstrate that *fur* mutations are necessary to render Δ*lpxC* nonessential and that deletion of *sspB* is not required for the viability of Δ*lpxC* cells. As in Δ*ctpA* Δ*fur* Δ*sspB*, the stable Δ*lpxC* Δ*fur* Δ*sspB* mutant still formed chains (Figure 1D), and xylose-driven *fur* expression induced lethality in this strain (Figure 3C).

Background levels of lipid A were detected in Δ*lpxC* Δ*fur* Δ*sspB* cells in the LAL assay (Figure 2A), strongly suggesting that lipid A is absent. To corroborate this result, we

extracted LPS species by three distinct methods, separated them by PAGE, and stained with Pro-Q Emerald 300. Hot aqueous phenol extracts of Δ*lpxC* Δ*fur* Δ*sspB* cells were deficient in S-LPS and putative lipid A +/− core (Figure 2B). However, unknown carbohydrate species were also extracted by this method. Extraction of free lipid A (El Hamidi et al., 2005) showed that a species of ~1,800 Da, consistent with the mass of *Caulobacter* lipid A (Smit et al., 2008), is present in NA1000 but absent from Δ*lpxC* Δ*fur* Δ*sspB* (Figure 2C, left). Again, however, unidentified carbohydrate species were present in these extracts. Last, the method of Darveau and Hancock (1983) yielded a single rough LPS species that was present in NA1000 and absent from Δ*lpxC* Δ*fur* Δ*sspB* (Figure 2C, right); this method yielded no unidentified contaminants. Although some *Caulobacter* extracts contain unidentified carbohydrates, these assays together strongly imply that lipid A is absent from the Δ*lpxC* Δ*fur* Δ*sspB* mutant. Xylose-driven expression of *lpxC* or *ctpA* restored the production of lipid A-containing species to Δ*lpxC* Δ*fur* Δ*sspB* or Δ*ctpA* Δ*CCNA_03733* Δ*sspB*, respectively (Figure 2D).

Lipid A extracts from Δ*ctpA* Δ*fur* Δ*sspB*, Δ*lpxC* Δ*fur* Δ*sspB*, and control strains were further analyzed by matrix-assisted laser desorption/ionization tandem mass spectrometry (MALDI-MS/MS). Wild-type NA1000, Δ*sspB*, and Δ*fur* Δ*sspB* extracts contained predominantly the full-length lipid A (*m/z* 1,874; Smit et al., 2008) and lesser amounts of an ion at *m/z* 1,858 that differs from 1,874 by 16 *m/z*, consistent with the absence of one hydroxyl group (Figures S3A–S3C). MALDI-MS analyses of lipid A extracts from Δ*ctpA* Δ*fur* Δ*sspB* cells revealed no ions consistent with full-length *Caulobacter* lipid A but identified ions at *m/z* 1,682 and *m/z* 1,486 (Figure S3D) that appeared to be missing the Gal*p*A residues at the 1 and 4′ positions. MS/MS analysis of these ions revealed losses of mass consistent with the loss of phosphates, as would be expected for the dissociation of canonical, phosphate-bearing lipid A structures. Although additional characterization is needed, our results suggest that *Caulobacter* mutants lacking CtpA produce a lipid A species that retains phosphate at the 1 and 4′ positions and lacks one or more of the secondary fatty acids. Although these lipid A species were detectable by MS, gel electrophoresis and LAL assays indicate that they are much less abundant than the lipid A in wild-type strains.

Lipid A extracts from the Δ*lpxC* Δ*fur* Δ*sspB* mutant yielded no ions consistent with wild-type lipid A and instead contained an unknown lipid (Figure S3E, *m/z* 1412). Numerous attempts to interpret the structure of this ion using the same type of tandem MS data as used in Figures S3A–S3D failed to generate a structural hypothesis resembling lipid A derivatives or other known lipids. Again, it is important to note that, although this unknown ion was detected by MS, gel electrophoresis and LAL assays together indicate that lipid A is absent from Δ*lpxC* Δ*fur* Δ*sspB* cells.

## Lipid A-deficient *Caulobacter* mutants produce a three-layer cell envelope

We analyzed NA1000, Δ*ctpA* Δ*fur* Δ*sspB*, and Δ*lpxC* Δ*fur* Δ*sspB* strains via electron cryotomography to assess the effects of mutations on cell envelope structure (Videos S1, S2, S3, and S4). As expected, the S-layer is absent from both mutants because of the loss of its O-antigen attachment site (Walker et al., 1994). Despite drastic reductions in lipid A levels, the Δ*ctpA* Δ*fur* Δ*sspB* and Δ*lpxC* Δ*fur* Δ*sspB* mutants still generate a three-layer

cell envelope with an OM (Figure 2E). Although much less severe than during acute CtpA depletion (Video S4), membrane blebs were often observed at the cell poles or division sites in Δ*ctpA* Δ*fur* Δ*sspB* and Δ*lpxC* Δ*fur* Δ*sspB* cells (Figure 2E). A large fraction of *ctpA* and *lpxC* mutant cells exhibited defects in stalk structure or internal membrane folds at the pole or midcell (n = 100; Δ*ctpA* Δ*fur* Δ*sspB*, 61%; Δ*lpxC* Δ*fur* Δ*sspB*, 51%; NA1000, 4%).

The ability to produce an OM in the absence of LPS, along with excess membrane folds in the cytoplasm, suggest that Δ*fur* could suppress Δ*ctpA* and Δ*lpxC* by increasing the synthesis of other lipids. We examined published transcriptomic data (Leaden et al., 2018; da Silva Neto et al., 2013) for a group of 22 genes predicted to participate in fatty acid or phospholipid synthesis. For 19 of these genes, expression was not altered in a Δ*fur* mutant or in wild-type cells treated with 2,2-dipyridyl to limit iron (Table S3). Of the three remaining genes, two were downregulated and one was upregulated only by iron limitation. Thus, Fur seems not to exert a direct or indirect transcriptional effect on genes related to lipid synthesis. However, post-transcriptional effects in Δ*fur* strains could cause an increase in production of lipids other than lipid A.

## Fur-regulated processes, rather than available iron levels, control the conditional essentiality of lipid A

LPS defects are usually associated with increased chemical sensitivity (Nikaido, 2003). Mutations in *fur* or O-antigen synthesis genes did not appreciably increase chemical sensitivity compared with NA1000, whereas strains lacking *ctpA* or *lpxC* had greater sensitivity to a subset of antibiotics and to all tested detergents (Figure 4A). In contrast, the Δ*lpxC* and Δ*ctpA* strains with suppressor mutations were much less susceptible to CHIR-090, an inhibitor of LpxC (McClerren et al., 2005; Figure 4B). We infer that suppressed Δ*lpxC* and Δ*ctpA* mutants are relatively insensitive to CHIR-090 because they already produce little lipid A or lack the target enzyme.

In agreement with its ability to suppress the lethality of Δ*lpxC* and Δ*ctpA*, Δ*fur* by itself greatly reduced the sensitivity of *Caulobacter* to CHIR-090 (Figure 4B). Fur is a widespread bacterial regulator of iron homeostasis that senses available $Fe^{2+}$ (Andrews et al., 2013; Fontenot et al., 2020). When bound to iron, Fur represses the transcription of genes for iron uptake and activates (directly or indirectly) the transcription of genes for iron-utilizing enzymes. Because iron is required for Fur-directed transcriptional regulation, we wanted to determine whether iron limitation could mimic the phenotypes of a Δ*fur* mutant. Culturing NA1000 with the iron chelator 2,2′-dipyridyl reduced its susceptibility to CHIR-090 to match that of the Δ*fur* mutant (Figure 4B). Neither depleting LpxC in *fur*$^{+}$ cells nor inducing *fur* in Δ*lpxC* Δ*fur* Δ*sspB* cells caused a reduction in viability in the presence of 2,2′-dipyridyl (Figures 4C and 4D). The NA1000, Δ*sspB*, and Δ*fur* Δ*sspB* strains cultured in 2,2′-dipyridyl retained LPS and lipid A +/− core (Figure 4E). Therefore, low iron availability does not induce loss of lipid A but is sufficient to maintain *Caulobacter* viability when lipid A is eliminated by chemical or genetic means.

Because they are impaired in iron sensing, *fur* mutants of other bacteria accumulate more available iron than the corresponding wild-type strains (Liu et al., 2020; Wofford et al., 2019). We measured available iron levels using a streptonigrin (SNG) sensitivity assay

(Justino et al., 2007; Nachin et al., 2001) because SNG killing is linked to intracellular formation of oxygen radicals in the presence of iron (Hassett et al., 1987; Yeowell and White, 1982). Growth of Δ*fur* and Δ*fur* Δ*sspB* cells was almost completely inhibited by 0.25 μg/mL SNG, whereas NA1000 was only mildly inhibited (Figure 4F), consistent with higher levels of available iron in Δ*fur* mutants. These findings indicate that excess available iron (in *fur* mutants) and iron depletion (by 2,2-dipyridyl) can support viability when lipid A synthesis is blocked chemically or genetically. Because *fur* deletion and iron chelation have the same effect on Fur-regulated gene expression but are predicted to have opposite long-term effects on Fur-independent iron signaling (Figure 4G), this implies that processes regulated by Fur in concert with iron are specifically responsible for survival of lipid A-deficient *Caulobacter* (Leaden et al., 2018; da Silva Neto et al., 2013).

## RB-TnSeq identifies sphingolipid synthesis genes needed for fitness when lipid A synthesis is chemically inhibited

To uncover additional factors that promote the survival of lipid A-deficient *Caulobacter*, we challenged an RB-TnSeq library constructed in NA1000 (Price et al., 2018) with CHIR-090. Individual barcode frequencies were measured by high-throughput sequencing before each trial and after growth in either PYE or PYE + 2 μg/mL CHIR-090, and we averaged and compared the gene fitness scores (Wetmore et al., 2015) from three trials under each condition (Figure 5A). We anticipated that mutations in *fur* would increase fitness in CHIR-090, but the RB-TnSeq library contained no insertions in *fur*. Surprisingly, nearly all genes known to be regulated by Fur (Leaden et al., 2018; da Silva Neto et al., 2013) had similar fitness scores in unstressed and CHIR-090-exposed cultures (Figure 5A).

Focusing on genes whose average fitness scores were 1 point or more lower in CHIR-090-treated cultures than in control cultures (Table S4), we identified five genes involved in sphingolipid synthesis: serine palmitoyltransferase (*spt*, *CCNA_01220*), acylcarrier protein (*acp*, *CCNA_01221*), ceramide reductase (*cerR*, *CCNA_01222*), ACP-synthetase (*acps*, *CCNA_01223*), and bacterial ceramide synthase (*bcerS*, *CCNA_01212*) (Olea-Ozuna et al., 2021; Stankeviciute et al., 2022). Fitness scores in CHIR-090 were also much lower for a neighboring operon of three uncharacterized genes predicted to modify lipids (*CCNA_01217-01219*; Marks et al., 2010; Figure 5A). None of these genes are known to be regulated by Fur or iron (Leaden et al., 2018; da Silva Neto et al., 2013). Using qPCR, we found that transcription of *CCNA_01217-01219* is unchanged in Δ*fur* Δ*sspB* and Δ*lpxC* Δ*fur* Δ*sspB* mutants (Figure 5B). As controls, *lpxC* transcripts were not detected in Δ*lpxC* Δ*fur* Δ*sspB* cells, and *bfd* (*CCNA_03372*) transcripts were significantly increased in both mutants, as observed previously (Figure 5B; Leaden et al., 2018).

To examine the roles of genes in the uncharacterized operon, we constructed unmarked deletions in the NA1000 and Δ*fur* Δ*sspB* backgrounds and complemented them with the corresponding genes expressed from the inducible *vanA* promoter (Thanbichler et al., 2007). Loss of *spt*, *CCNA_01217*, *CCNA_01218*, or *CCNA_01219* greatly increased the susceptibility to CHIR-090, either in NA1000 or in Δ*fur* Δ*sspB* cells (Figure 5C), and expression of the complementing gene from the *vanA* locus restored the parental level of susceptibility, validating the RB-TnSeq results.

Mutations in *CCNA_01217-01219* or *spt* could increase CHIR-090 sensitivity in two different ways: by damaging the cell's permeability barrier and giving easier access to CHIR-090 or by making it more difficult for cells to grow after lipid A synthesis is inhibited. To eliminate changes in drug access as a factor in the experiment, we measured the effects of *CCNA_01217*, *CCNA_01218*, and *spt* on cell viability when LpxC was depleted. We deleted individual genes in the strain Δ*lpxC* Δ*fur* Δ*sspB* + P*xyl-lpxC*::*3xFLAG*::*ssrA* (KR4091) and complemented them with *vanA*-driven copies as described above. The parent strain lacks *fur* and grows in PYED (with or without vanillate) when LpxC is depleted. In contrast, KR4091 lacking *CCNA_01217*, *CCNA_01218*, or *spt* grew poorly in PYED, and growth was fully or partially restored by expressing the complementing gene from the vanillate promoter (Figure 5D). Because this assay does not rely on an exogenous inhibitor of LpxC, we conclude that *CCNA_01217-8* and *spt* are critical for the fitness of lipid A-deficient *Caulobacter*, not simply for exclusion of CHIR-090.

KR4091 lacking *CCNA_01218* grew poorly in PYEX medium without vanillate, where *lpxC* is transcribed (Figure 5D), and we were unable to isolate a stable derivative of KR4091 harboring Δ*CCNA_01219* and *vanA*::*01219*. These findings could indicate that Δ*CCNA_01218* and Δ*CCNA_01219* have a negative genetic interaction with Δ*fur* and/or Δ*sspB*. However, we detected no significant additive growth phenotypes when Δ*CCNA_01218* or Δ*CCNA_01219* was combined with Δ*fur* Δ*sspB* in strains where LpxC was expressed from the native locus (Figure 5E). We therefore favor the hypothesis that Δ*CCNA_01218* or Δ*CCNA_01219* is particularly detrimental in the highly modified KR4091 background, where *fur* and *sspB* are absent, and an epitope-tagged version of LpxC is expressed from a nonnative promoter.

## CCNA_01217-01219 convert neutral ceramide to an anionic sphingolipid, ceramide phosphoglycerate

The importance of Spt for viability in the absence of lipid A indicated a role for sphingolipids in this phenotype. Because *Sphingomonas* spp. produce anionic glycosphingolipids (GSLs) on the OM (Kawasaki et al., 1994), we initially hypothesized that *Caulobacter* responds to *lpxC* deletion by upregulating GSL production. The *Caulobacter* sphingolipid glycosyltransferases Sgt1 and Sgt2 are expressed specifically under phosphate-limiting conditions (Stankeviciute et al., 2019), and their transcripts were not upregulated in Δ*fur* Δ*sspB* or Δ*lpxC* Δ*fur* Δ*sspB* cells grown in PYE (Figure 5B). Transposon insertions in *sgt1* or *sgt2* did not reduce the fitness of CHIR-090-treated cells in RB-TnSeq. Thus, although Sgt1 and Sgt2 are not critical in these experiments, they may be important for the fitness of lipid A-deficient *Caulobacter* under other conditions.

A careful analysis of the *Caulobacter* lipidome revealed two related anionic sphingolipid species: ceramide phosphoglycerate (CPG) and ceramide containing two phosphoglycerate moeities (CPG2) (Figure 6A). Liquid chromatography (LC)-MS/MS analysis confirmed the proposed structures of these lipids (Figure 6B). To determine whether *CCNA_01217-01219* are involved in CPG/CPG2 synthesis, we analyzed lipid extracts from mutant and complemented mutant strains. Δ*CCNA_01218* cells lacked ceramide phosphate, CPG, and CPG2 but retained neutral ceramide (Figure 6C). CCNA_01218 is annotated as a

sphingosine kinase-related protein and has a conserved LCB5 domain (Nagiec et al., 1998). Thus, we propose that CCNA_01218 (hereafter CpgB) adds the initial phosphate on the ceramide (Figure 6D). Δ*CCNA_01219* cells lacked CPG and CPG2 but retained ceramide phosphate and neutral ceramide (Figure 6C). This is consistent with CCNA_01219 (hereafter CpgC) adding a glycerate molecule to ceramide phosphate to form CPG (Figure 6D). CCNA_01219 has no conserved domains, and a BLAST analysis identified homologs only in Caulobacterales and Sphingomonadales. Δ*CCNA_01217* cells lacked CPG2 but retained CPG, ceramide phosphate, and neutral ceramide (Figure 6C). CCNA_01217 has a conserved phosphatidylglycerophosphate synthase (PgsA) domain that is normally involved in phosphatidylglycerol (PG) synthesis. PG is the dominant phospholipid in *Caulobacter* membranes (Stankeviciute et al., 2019), but the essential PgsA ortholog *CCNA_03002* is likely responsible for its synthesis (Christen et al., 2011; Marks et al., 2010). Thus, we conclude that CCNA_01217 (hereafter CpgA) adds a second phosphoglycerate to CPG to form CPG2 (Figure 6D). Each phenotype was complemented by expressing the respective gene from a vanillate-inducible promoter (Figure 6C).

CPG/CPG2 species appear to be a relatively small percentage of the total lipidome (Figure S4), raising the question of how these lipids support viability in the absence of lipid A. The CPG2 molecule is very polar, as evidenced by its very long LC retention time, and we hypothesize that this lipid is not efficiently extracted by standard methods. Although we tried several modifications to increase the extraction yield, we made only marginal improvements. Our genetic data show that CpgA adds the second phosphoglycerate molecule to generate CPG2, but we cannot rule out the possibility of higher-order polymers containing additional phosphoglycerates, which would be even more polar and difficult to extract.

## CPG mediates susceptibility to colistin

CAMPs have been demonstrated to kill Gram-negative bacteria by first interacting with negatively charged groups on surface-exposed LPS. Phosphates at the 1 and 4′ positions of lipid A are particularly important for this interaction, and several bacteria possess mechanisms to modify them, reducing the negative surface charge and CAMP sensitivity (Moffatt et al., 2019; Velkov et al., 2010). Despite lacking phosphate groups on its lipid A, *Caulobacter* is highly sensitive to colistin, and the antimicrobial effect is retained in the lipid A-deficient strain Δ*lpxC* Δ*fur* Δ*sspB* (Figure 7A). Because CPG and CPG2 are anionic, we considered whether they may be the colistin target in *Caulobacter*. Indeed, colistin failed to inhibit the growth of mutants lacking *cpgA*, *cpgB*, or *cpgC* (Figure 7A). Because deletion of *cpgA*, catalyzing conversion of CPG to CPG2, can alone greatly reduce colistin sensitivity, and because elimination of lipid A had no effect, we infer that a primary target of colistin on the *Caulobacter* surface is CPG2. These findings are consistent with our hypothesis that CPG lipids are a significant component of the outer leaflet of the OM whose detection is limited by inefficient extraction.

# DISCUSSION

## CtpA is required for wild-type lipid A structure and abundance

We performed a suppressor screen to discover the essential function of CtpA, which contains active-site residues characteristic of tyrosine phosphatases. Inactivation of *fur* or genes involved in O-antigen synthesis permitted deletion of *ctpA* and yielded cells with drastically reduced amounts of lipid A. MS/MS analysis of the remaining lipid A extracted from Δ*ctpA* Δ*fur* Δ*sspB* cells was consistent with species that retain phosphoryl groups at the 1 and 4′ positions of the central disaccharide, suggesting that CtpA is responsible for dephosphorylating at least one of these positions in preparation for addition of Gal*p*A residues.

Some alphaproteobacteria produce lipid A species with a trior tetrasaccharide backbone (De Castro et al., 2008). In *Rhizobia*, the phosphatases LpxE and LpxF dephosphorylate the 1 and 4′ positions, respectively, of lipid A at the periplasmic surface of the IM (Karbarz et al., 2003; Wang et al., 2006). Sugars are then added to the 1 and 4′ positions by the glycosyltransferases RgtF and RgtD, respectively, before transport of mature LPS to the OM (Brown et al., 2012, 2013). NA1000 harbors a gene (*CCNA_03113*) with similarity to *lpxE* but none with similarity to *lpxF*, raising the possibility that CtpA substitutes for LpxF. Additional work is needed to test this hypothesis and to understand how mutations in *ctpA* affect lipid A abundance.

## *Caulobacter* requires anionic sphingolipids to survive without lipid A

The enzyme LpxC and lipid A itself are dispensable for viability in *C. crescentus*, conditional on the absence of Fur and the presence of anionic sphingolipids (CPG/CPG2) (Figure 7B). LPS molecules form a robust permeability barrier based on (1) tight packing of the six saturated acyl chains of lipid A and (2) a lateral network formed by bridging of the phosphate groups on lipid A + core by divalent cations such as $Mg^{2+}$ and $Ca^{2+}$ (Nikaido, 2003). *Caulobacter* lipid A and core oligosaccharide lack phosphate groups that would participate in a lateral ionic network (Smit et al., 2008). We propose that negative charges on CPG/CPG2 provide this function in the *Caulobacter* OM, accounting for the observation that *cpgABC* and other sphingolipid synthesis genes are important for fitness even when LPS is present (Figure 5A; Christen et al., 2011). Evidence that CPG/CPG2 contribute a negative charge to the OM comes from studies of CAMP sensitivity. We previously observed that Spt is necessary for susceptibility to polymyxin B, but Sgt1 and Sgt2, which convert neutral ceramide to the anionic species GSL-2, are not required (Stankeviciute et al., 2019). This result was puzzling because neutral ceramide was not expected to be a target for CAMP activity. Here we provide an explanation by showing that neutral ceramide is converted by CpgABC to a different anionic species, CPG2, and that this lipid, rather than LPS, is critical for colistin susceptibility.

## Inhibition of Fur-mediated gene expression is necessary to survive in the absence of lipid A

In contrast to *Sphingomonas* spp., the presence of cell surface sphingolipids is not sufficient for *Caulobacter* to survive without lipid A. In addition, Fur must be deactivated. Iron

limitation (via growth in 2,2-dipyridyl) and excess available iron (because of disruption of iron homeostasis in Δ*fur*) supported the viability of lipid A-deficient *Caulobacter*. These results imply that genes or processes regulated by Fur in complex with iron, rather than those regulated by iron independent of Fur, are the critical factors.

Fur controls iron homeostasis in *Caulobacter* by directly or indirectly regulating ~120 genes (Leaden et al., 2018; da Silva Neto et al., 2009, 2013). A significant fraction of the Fur regulon, comprising 45 genes, is predicted to encode membrane proteins functioning in transport reactions or energy metabolism. *Caulobacter* Fur represses the transcription of genes for iron uptake and activates the expression of genes encoding iron-containing proteins, such as cytochromes and enzymes harboring Fe/S clusters. Fur is linked to oxygen signaling in *Caulobacter* by activating the transcription of *fixK*, which mediates the response to hypoxia (Crosson et al., 2005). In addition, the Δ*fur* mutant has a constitutively elevated level of intracellular oxidation and displays impaired growth under oxidative stress, implicating Fur in prevention of oxidative stress (da Silva Neto et al., 2009; Leaden et al., 2018).

Our *ctpA* suppressor screen retrieved mutations in *fur* but not in genes whose transcription is activated by Fur. Thus, it is unlikely that there is a singular Fur-activated gene whose expression is lethal when lipid A is depleted. Consistently, RB-TnSeq revealed that no transposon insertions in Fur-activated genes led to significantly increased fitness during challenge with CHIR-090. Because mutations would be more likely to cause loss than gain of function, we might not retrieve suppressors that work by increasing gene expression or activity. However, if there were a singular Fur-repressed gene whose upregulation was required to render lipid A dispensable, then transposon insertions in this gene would be expected to reduce the fitness of CHIR-090-treated cells. Again, no individual gene fits this profile, but one caveat is that essential genes are excluded from RB-TnSeq analysis.

Mutations in *fur* could therefore support the viability of lipid A-deficient *Caulobacter* via (1) downregulation of multiple Fur-activated genes, (2) upregulation of multiple Fur-repressed genes, and/or (3) activation of compensatory cellular stress responses. Because Fur regulates the expression of many OM and IM proteins (da Silva Neto et al., 2009; Leaden et al., 2018), deletion of *fur* could alter envelope composition in a manner that renders lipid A nonessential. Alternatively, the transcriptional changes and oxidative stress that follow *fur* deletion could activate a network of stress responses that together make it possible to survive in the absence of lipid A.

## Principles governing lipid A essentiality

Hypotheses to explain the essential nature of lipid A include its chemical barrier function, detrimental activation of stress responses when it is depleted, its role in OM protein biogenesis or function, and its mechanical role in resisting turgor pressure (Rojas et al., 2018; Zhang et al., 2013). *Caulobacter* is only the fourth LPS-bearing Gram-negative bacterium demonstrated to survive in the absence of lipid A, following *N. meningitidis*, *M. catarrhalis*, and *A. baumannii*. So far, however, no single theme has emerged to explain why this select and phylogenetically diverse group of Gram-negative bacteria is capable of surviving without lipid A.

In *A. baumannii*, proteins that synthesize PG in lateral cell walls (the elongasome) are critical for the fitness of lipid A-deficient strains, suggesting that alterations in PG structure are needed to compensate for the OM's loss of mechanical strength (Simpson et al., 2021). Because elongasome components are essential for viability in *Caulobacter* (Christen et al., 2011), RB-TnSeq could not reveal their fitness effects in CHIR-090-treated cultures. Lipid A-deficient strains of *A. baumannii* consistently display increases in expression of lipoproteins and the Lol pathway for lipoprotein transport to the OM (Boll et al., 2016; Henry et al., 2015). Two lipoprotein synthesis genes, *lgt* (*CCNA_00525*) and *lnt* (*CCNA_00050*), had markedly reduced fitness scores in CHIR-090-treated *Caulobacter* cultures compared with unstressed cultures, so OM lipoproteins may help to compensate for the absence of lipid A in diverse species.

*A. baumannii ΔlpxC* mutants have growth and morphological defects that are corrected when the growth rate is limited by environmental factors, such as low temperature or nutrient limitation (Nagy et al., 2019), suggesting that one barrier for elimination of lipid A is the rate of synthesis of alternative molecules to constitute the OM. Although Δ*fur* slows the growth of *Caulobacter* (Figure S1; Table S5; da Silva Neto et al., 2009), we found that slow growth in PYE at a reduced temperature was not sufficient to support the viability of *fur*$^{+}$ *Caulobacter* depleted of LpxC (Figure S5A) or of Δ*lpxC* Δ*fur* Δ*sspB* cells with *fur* expression restored (Figure S5B). If slow growth were sufficient to render lipid A nonessential, then our screen for *ctpA* suppressors should have retrieved a wider variety of mutations that slow *Caulobacter* growth rather than repeated mutations in *fur* and genes for O-antigen synthesis. Although a reduced growth rate may play a role, we propose that the Δ*fur* mutation provides specific, unknown benefits that support viability in the absence of lipid A.

Our work suggests that possession of genes to produce anionic sphingolipids may provide certain Gram-negative bacteria with an unusual capacity to survive without lipid A. Anionic sphingolipids can also underlie clinically important phenotypes in wild-type membranes that retain LPS, such as susceptibility to CAMPs, which are used as a last line of defense against multi-drug-resistant infections. Thus, functions traditionally attributed to lipid A may be performed wholly or in part by alternative lipids, underscoring the need to study lipid A functions in diverse species and to identify and functionally characterize novel lipids.

## Limitations of the study

Because lipid A-deficient strains (Δ*lpxC* or Δ*ctpA*) were not accessible by double homologous recombination, we used LpxC or CtpA depletion strains as an intermediate step in strain construction. As a result, the lipid A-deficient strains in this study lack SspB, an adaptor for ClpXP-mediated degradation of ssrA-tagged proteins (Chien et al., 2007; Levchenko et al., 2000). Although Δ*sspB* is not required for survival of Δ*lpxC* strains (Table S2), this allele may affect phenotypes via changes in protein quality control (Keiler et al., 1996).

*Caulobacter* contains unknown glycosylated molecules that are co-extracted with lipid A or LPS (Figures 2B and 2C). Because all extracts were treated with Proteinase K, it is unlikely that these molecules are glycoproteins. *Caulobacter* synthesizes several

glycosylated diacylglycerol species (Stankeviciute et al., 2019), which could account for these gel bands. Similarly, an ion present in lipid A extracts of Δ*lpxC* Δ*fur* Δ*sspB* cells (Figure S3E) could not be identified by MS/MS. Although the LAL assay results indicate that these species are not lipid A derivatives, our data do not prove this definitively.

Our study identifies a major function of CPG/CPG2 in supporting the viability of lipid A-deficient *Caulobacter*, but we only detect small amounts of these lipids in Bligh-Dyer extracts (Figure S4). We hypothesize that the highly polar nature of CPG/CPG2 makes them difficult to extract and that they are more abundant than they appear; however, we have no direct evidence of this. We also propose, based on the reduced colistin sensitivity of *cpgABC* mutants (Figure 7A), that CPG/CPG2 are present in the outer leaflet of the OM, similar to the sphingolipids in *Sphingomonas* spp. (Kawasaki et al., 1994). Colistin disrupts the OM by interacting with surface-exposed LPS, but this is not sufficient to kill Gram-negative bacteria (MacNair et al., 2018). Instead, colistin kills by interacting with LPS molecules that are in the IM en route to the cell surface (Sabnis et al., 2021). By analogy, CPG/CPG2 could theoretically confer colistin susceptibility on *C. crescentus* while remaining in the IM.

## STAR★METHODS

Detailed methods are provided in the online version of this paper and include the following:

### RESOURCE AVAILABILITY

#### Lead contact

- Further information and requests for resources and reagents should be directed to and will be fulfilled by the lead contact, Kathleen R. Ryan (krr@berkeley.edu).

#### Materials availability

- All unique/stable reagents generated in this study are available from the lead contact upon request, but we may require a payment and/or a materials transfer agreement if there is potential for commercial application.

#### Data and code availability

- Genome sequence data have been deposited at the Sequence Read Archive at https://www.ncbi.nlm.nih.gov/sra and are publicly available as of the date of publication. Accession numbers are listed in the key resources table. RB-TnSeq data have been deposited at https://fit.genomics.lbl.gov/ and are publicly available as of the date of publication. Accession numbers are listed the key resources table. LC/MS data analyzing sphingolipids have been deposited at Mendeley Data and are publicly available as of the date of publication. DOIs are listed in the key resources table. LC-MSMS data analyzing lipid A species have been deposited at Mendeley Data and are publicly available as of the date of publication. DOIs are listed in the key resources table. This paper analyzes existing, publicly available data, whose sources are listed in the key resources table. Microscopy and gel electrophoresis images will be shared by the lead contact upon request.

- This paper does not report original code.
- Any additional information required to reanalyze the data reported in this paper is available from the lead contact upon request.

## EXPERIMENTAL MODEL AND SUBJECT DETAILS

All *Caulobacter crescentus* strains were derived from NA1000 (Evinger and Agabian, 1977) and are listed in Table S6. *Caulobacter* was grown in peptone-yeast extract medium (PYE, Ely, 1991) at 30°C. PYE was supplemented with 0.3% xylose (PYEX) or 0.2% dextrose (PYED) where indicated. When changing between inducing and non-inducing conditions, cells were washed twice with PYE medium lacking supplemental sugars or vanillate before being released into or plated on medium with a different supplement. Counter-selection using *sacB* was performed using 3% sucrose. 100 μM 2,2′-dipyridyl was added to culture media to achieve low-iron conditions. Vanillic acid was added to PYE media at final concentrations of 0.5 mM (plate assays) or 0.1 mM (liquid assays) to drive gene expression from the *vanA* promoter. Antibiotics added to PYE were used at the following concentrations (μg/mL) for liquid (L) or solid (S) medium: kanamycin, 5 (L), 25 (S); chloramphenicol, 1 (L/S); nalidixic acid, 20 (S); gentamycin, 25 (L), 5 (S); oxytetracycline, 1 (L), 2 (S); spectinomycin, 25 (L), 100 (S); hygromycin, 100 (L/S); streptonigrin 0.025 or 0.25 (L). *E. coli* strains were grown in lysogeny broth (10 g/L tryptone, 5 g/L yeast extract, 5 g/L NaCl) at 37°C, supplemented with antibiotics at the following concentrations (μg/mL) for liquid (L) or solid (S) medium: kanamycin, 30 (L), 50 (S); chloramphenicol, 20 (L), 30 (S); gentamicin, 15 (L), 20 (S); tetracycline, 12 (L/S); spectinomycin, 50 (L/S); hygromycin, 100 (L/S). Diaminopimelic acid (0.3 mM) was added to solid or media to support the growth of *E. coli* strain WM3064 (Dehio and Meyer, 1997).

## METHOD DETAILS

**Plasmid construction—**Plasmid descriptions are listed in Table S7. Primer sequences used for plasmid construction are listed in Table S8. Gibson assembly was performed using vectors linearized with restriction enzymes, DNA fragments amplified with Q5 High-Fidelity DNA Polymerase, and NEBuilder HiFi DNA Assembly Master Mix.

**pZIK133:** The LpxC depletion vector was constructed by placing the *lpxC* coding region, C-terminally fused to a 3xFLAG tag (amino acid sequence: DYKDHDGDYKDHDIDYKDDDDK) followed by the *Caulobacter* ssrA tag (amino acid sequence: AANDNFAEEFAVAA), under control of the *xylX* promoter. The *xylX* promoter was amplified using the pJS14-PxylX and PxylX-lpxC R primers. The PxylX-lpxC F and lpxC-3xFLAG R primers were used to amplify *lpxC*. The C-terminal fusion was amplified from pAB6 using the lpxC-3xFLAG F and ssrA-pJS14 primers. The final plasmid was assembled via Gibson cloning into a BamHI/EcoRI-digested pJS14 backbone.

**pZIK134:** For the *lpxC* knockout construct, flanking homology regions were amplified using the primers lpxC UpF and lpxC UpR for the 5′- region, and lpxC DownF and lpxC DownR for the 3′- region. The 5′- arm included a 5′- SpeI site and a 3′- EcoRI site, and the 3′- arm included a 5′- EcoRI site and a 3′- SphI site. These fragments were digested with

the indicated enzymes and ligated into SpeI/SphI-digested pNPTS138. This intermediate plasmid was linearized with EcoRI, and the EcoRI-digested *tetAR* cassette from pKOC3 was inserted to make the final construct.

**pZIK73 and pZIK78:** For knockouts of *CCNA_01553* or *CCNA_00497*, flanking homology regions were amplified using the following primer pairs: pZIK73 5′- region (01553 UpF; 01553 UpR), pZIK73 3′- region (01553 DownF; 01553 DownR), pZIK78 5′- region (00497:hyg UpF; 00497:hyg UpR), pZIK78 3′- region (00497:hyg DownF; 00497:hyg DownR). For each construct, the 5′- arm included a 5′- SpeI site and a 3′- SmaI site, and the 3′- arm included a 5′- SmaI site and a 3′- EcoRI site. These fragments were digested with the indicated enzymes and ligated into SpeI/EcoRI-digested pNPTS138. The intermediate plasmids were linearized with SmaI, and the SmaI-digested *hyg* cassette from pHP45Ω-hyg was inserted to make the final constructs.

**pZIK80, pZIK81, pZIK82, and pZIK161:** For the knockouts of *CCNA_03733*, *CCNA_01068*, *CCNA_01055*, or *CCNA_00055*, flanking homology regions were amplified using the following primer pairs: pZIK80 5′- region (03733:hyg UpF; 03733:hyg UpR), pZIK80 3′- region (03733:hyg DownF; 03733:hyg DownR), pZIK81 5′- region (01068:hyg UpF; 01068:hyg UpR), pZIK81 3′- region (01068:hyg DownF; 01068:hyg DownR), pZIK82 5′- region (01055:hyg UpF; 01055:hyg UpR), pZIK82 3′- region (01055:hyg DownF; 01055:hyg DownR), pZIK161 5′- region (fur UpF; fur UpR), pZIK161 3′- region (fur DownF; fur DownR). Each 5′- arm included a 5′- SpeI site and a 3′- BamHI site, and each 3′- arm included a 5′- BamHI site and a 3′- EcoRI site. These fragments were digested with the indicated enzymes and ligated into SpeI/EcoRI-digested pNPTS138. The intermediate plasmids were linearized with BamHI, and the BamHI-digested hyg cassette from pHP45Ω-hyg was inserted to make the final constructs.

**pZIK172-174:** *CCNA_00497*, *CCNA_01553*, *or CCNA_03733* were placed under control of the *xylX* promoter on pXCERN-2, which integrates at the *xylX* promoter. The corresponding genes were initially cloned into pVCERN-2 before being moved into pXCERN-2. Genes were amplified with the following primer pairs: *CCNA_00497* (pVCERN-2 00497 F; pVCERN-2 00497 R), *CCNA_01553* (pVCERN-2 01553 F; pVCERN-2 01553 R), *CCNA_03733* (pVCERN-2 03733 F; pVCERN-2 03733 R). Primer sets replace the start codon with an NdeI site and add a SacI site after the stop codon. The corresponding gene fragment and pVCERN-2 were digested with NdeI and SacI and ligated together. An NdeI/MluI fragment was subsequently excised from each vector and moved to pXCERN-2 cut with the same enzymes.

**pZIK175:** *CCNA_00055* (*fur*) was placed under control of the *xylX* promoter on pXCERN-2, which integrates at the *xylX* promoter. *CCNA_00055* was initially cloned into pVCERN-2 before being moved into pXCERN-2. *CCNA_00055* was amplified using the Pvan-fur and fur-pVCERN primers, and this fragment was inserted into NdeI/SacI-digested pVCERN-2 via Gibson assembly. The NdeI/MluI fragment was subsequently excised and ligated into NdeI/MluI-digested pXCERN-2.

**pGS74 and pGS76:** For markerless deletions of *CCNA_01217* or *CCNA_01219*, 5′- and 3′- flanking homology regions, respectively, were amplified using the primer pairs EK1047/1048 and EK1049/1050 (*CCNA_01217*) and EK1055/1056 and EK1057/1058 (*CCNA_01219*). pNPTS138 was amplified with primers EK897/898, and vectors were constructed by Gibson assembly.

**pKR429:** For markerless deletion of *CCNA_01218*, 5′- and 3′- flanking homology regions, respectively, were amplified using the primer pairs 01218 up_fwd/01218 up_rev and 01218 down_fwd/01218 down_rev. pNPTS138 was digested with EcoRI and HindIII, and the vector was constructed by Gibson assembly.

**pEK406:** For complementing the deletion of *CCNA_01217* in LC-MS/MS experiments, *CCNA_01217-FLAG* was amplified using primers EK1357/1358. The PCR product was ligated into the NdeI/NheI sites of pVCHYC-5.

**pKR432–434:** For appending a C-terminal FLAG tag to the *CCNA_01218-20* open reading frames. The indicated genes were amplified from NA1000 genomic DNA using primer pairs Nde-01218/01218-Mlu, Nde-01219/01219-Mlu, or Nde-01220/01220-Mlu. Fragments were digested using NdeI/MluI and ligated into pFLGC-1 digested with the same enzymes.

**pKR435:** For expressing *CCNA_01218-FLAG* from the chromosomal *vanA* promoter. *CCNA_01218-FLAG* was amplified from pKR432 using primers 01218-FLAG F/01218-FLAG R and inserted in NdeI-digested pVGFPC-2 by Gibson assembly.

**pKR436:** For expressing *CCNA_01219-FLAG* from the chromosomal *vanA* promoter. *CCNA_01219-FLAG* was amplified from pKR433 using primers 01219-FLAG F/01219-FLAG R and inserted in NdeI-digested pVGFPC-2 by Gibson assembly.

**pKR437:** For expressing *CCNA_01220-FLAG* from the chromosomal *vanA* promoter. *CCNA_01220-FLAG* was amplified from pKR434 using primers 01220-FLAG F/01220-FLAG R and inserted in NdeI-digested pVGFPC-2 by Gibson assembly.

**pKR438:** For expressing *CCNA_01217-FLAG* from the chromosomal *vanA* promoter. *CCNA_01217-FLAG* was amplified from pEK406 using primers 01217-FLAG F/01217-FLAG R and inserted in NdeI-digested pVGFPC-4 by Gibson assembly.

**Strain construction—**Unless otherwise stated, plasmids were mobilized from *E. coli* into *C. crescentus* by conjugation. *E. coli* donors were counterselected by the addition of nalidixic acid, or when WM3064 was used as the donor, by omitting diaminopimelic acid from selection plates. Gene deletion or disruption was achieved by two-step homologous recombination using *sacB* counterselection (Ely, 1991).

**LpxC depletion strain—**The LpxC depletion strain KR4007 was constructed in a parallel manner to the CtpA depletion strain KR3906. pZIK133 was introduced to KR1499 (Δ*sspB*) by conjugation and selection on PYE/chloramphenicol. pZIK134 was conjugated into this intermediate strain, and colonies were selected on PYEX/chloramphenicol/oxytetracycline.

After *sacB* counterselection on PYEX/sucrose/oxytetracycline, colonies were screened for chloramphenicol$^R$ kanamycin$^S$ on PYEX.

**Stable Δ*ctpA* or Δ*lpxC* strains—**To generate stable Δ*ctpA* or Δ*lpxC* strains without covering plasmids, candidate suppressor genes identified by screening were disrupted in KR3906 or KR4007, respectively, using two-step homologous recombination while cultivating the cells on PYEX. Intermediate strains (sucrose$^R$ hygromycin$^R$ kanamycin$^S$) were grown in liquid PYED without chloramphenicol to permit loss of the *ctpA* or *lpxC* covering plasmid, plated on PYED, and tested for chloramphenicol$^S$. Absence of *ctpA* was confirmed using primers ctpA KO F and ctpA KO R, and absence of *lpxC* was confirmed using primers lpxC KO F and lpxC KO R. The genomes of Δ*ctpA* Δ*fur* Δ*sspB* (KR4102) and Δ*lpxC* Δ*fur* Δ*sspB* (KR4103) were resequenced and contained no additional mutations. Stable Δ*ctpA* or Δ*lpxC* strains were further modified by electroporation with purified plasmids (Gilchrist and Smit, 1991) to restore xylose-driven suppressor gene expression.

**Deletions of sphingolipid synthesis genes—**Deletions in *CCNA_01217*, *CCNA_01218*, *CCNA_01219*, and *CCNA_01220* in NA1000 or KR4077 were made by conjugation of the appropriate pNPTS138-based plasmid, followed by selection on PYE/kanamycin/nalidixic acid. After overnight growth in PYE, cells were plated on PYEX/sucrose, and sucrose$^R$ colonies were screened for kanamycin$^S$. Colony PCR with the following primers was used to detect the deletion of the indicated chromosomal genes: *CCNA_01217*, EK S238/S239; *CCNA_01218*, EK S240/S241; *CCNA_01219*, EK S242/S243; *CCNA_01220*, EK S216/S217. Loci were sequenced with the indicated primers to ensure the accuracy of in-frame deletions. Unmarked deletions of *CCNA_01217*, *CCNA_01218*, *CCNA_01219*, and *CCNA_01220* were made in KR4091 by conjugation of KR4091 with WM3064 harboring the appropriate pNPTS138-based plasmids, followed by selection on PYEX/kanamycin medium omitting diaminopimelic acid. After growth overnight in PYEX, cells were plated on PYEX/sucrose, and sucrose$^R$ colonies were screened for kanamycin$^S$. Colony PCR with the following primers was used to detect the deletion of the indicated chromosomal genes: *CCNA_01217*, EK S238/S239; *CCNA_01218*, EK S240/S241; *CCNA_01219*, EK S242/S243; *CCNA_01220*, EK S216/S217. Loci were sequenced with the indicated primers to ensure the accuracy of in-frame deletions. Strains were screened for oxytetracycline$^R$ and hygromycin$^R$ to ensure that they maintained deletions of *lpxC* and *fur*, respectively.

**Complementation of *spt* and *cpg* genes—**To complement deletions of *CCNA_01217-01220*, the following plasmids were introduced by conjugation to place the complementing gene under control of the chromosomal *vanA* promoter: Δ*CCNA_01217*, pEK406 (for LC-MS studies) or pKR438 (for growth and chemical sensitivity assays); Δ*CCNA_01218*, pKR435; Δ*CCNA_01219*, pKR436; or Δ*CCNA_01220*, pKR437. When introducing plasmids into strains capable of *lpxC* depletion (based on KR4091), plasmids were delivered from WM3064 to avoid the use of multiple antibiotics for selection/counterselection. Correct integration of plasmids at the *vanA* locus was confirmed by colony PCR using primers RecUni-1 and RecVan-2 (Thanbichler et al., 2007).

**Suppressor selection—**KR3906 was grown to full density in PYEX. 300 μL of culture was transferred onto an open, sterile Petri dish and mutagenized in a UV Stratalinker 1800 (Stratagene) with 30,000 μJ of energy. Mutagenized cells were plated on PYED. Recovered colonies were grown in liquid PYED overnight to allow loss of the covering plasmid, and samples were streaked onto PYED. Isolated colonies were screened for chloramphenicol sensitivity. $Chlor^S$ isolates were grown in PYE and saved at −80°C in 10% dimethylsulfoxide. Loss of *ctpA* was confirmed via PCR using the primers ctpA KO F and ctpA KO R, which anneal to the interior of the open reading frame.

**Genome resequencing—**Strains were grown to full density in PYE, and genomic DNA was extracted using the DNeasy Blood & Tissue Kit (Qiagen). Genomic DNA was submitted to the UC Berkeley Functional Genomics Laboratory, where libraries were prepared using a PCR-free protocol with multiplexing (http://qb3.berkeley.edu/gsl/). Samples were sequenced at the UC Berkeley Vincent J. Coates Genomics Sequencing Laboratory using a 300PE or 150PE MiSeq v3 run. Genomic sequencing data were analyzed for variants using the Galaxy platform at usegalaxy.org (Afgan et al., 2016). Adapter sequences were removed using Cutadapt (Martin, 2011), and sequences were aligned to the NA1000 genome (Marks et al., 2010) using Bowtie2 (Langmead and Salzberg, 2012). FreeBayes (Garrison and Marth, 2012) was used to analyze the BAM files for variants. Variants with quality scores below 300 were discarded as noise.

**qRT-PCR assays—**RNA from mid-log phase cells was extracted with the RNeasy kit (Qiagen). Purified RNA was treated with DNase (Thermo Scientific) to remove any contaminating DNA, and the RNA was re-purified using the RNeasy kit to remove the DNase. RNA concentrations were measured on a Nanodrop and normalized to 10 ng/μL. The RNA was reverse-transcribed with the High Capacity cDNA Reverse-Transcription Kit (Thermo Scientific). qRT-PCR was performed with technical duplicate and biological triplicate samples on a QuantStudio 6 instrument (Thermo Scientific) using the PowerUP SYBR Green master mix (Thermo Scientific) and 300 nM primers (Table S8). Relative expression was determined by the relative ΔΔCt method (Livak and Schmittgen, 2001) and normalized to *rpoD* expression.

**Growth and viability assays—**For plate assays, strains were grown to $OD_{660}$ = 0.2–0.5 in permissive media, washed twice in PYE medium with no additions, and diluted to $OD_{660}$ = 0.1. 10 μL drops of ten-fold serial dilutions were pipetted onto permissive and nonpermissive media. Plates were incubated for 3 days at 30°C, and images are representative of at least three independent trials. For endpoint growth assays in liquid media, strains were grown in permissive media to $OD_{660}$ = 0.2–0.5. After washing in PYE medium without additions, cells were resuspended at $OD_{660}$ = 0.01 in permissive and nonpermissive media. $OD_{660}$ values were measured after 24 h growth at 30°C. Growth curves where $OD_{660}$ and colony forming units (cfu)/ml were measured at 3h intervals were performed using 3–4 mL cultures shaken at 250 rpm in a 30°C incubator. Growth curves where $OD_{660}$ was measured every 15 min were performed in a BioTek Epoch2 microplate reader held at 30°C with constant shaking at 567 cpm between reads.

**Disc diffusion assays—**Cultures were grown to mid-exponential phase ($OD_{660}$ 0.2–0.5), and an amount of cells equivalent to 250 μL of culture at $OD_{660}$ = 0.2 was added to 4 mL of PYE swarm agar (0.3% w/v agar) pre-warmed to 42°C. Swarm agar containing bacteria was spread onto solid PYE and allowed to set. Antibiotics or detergents (10 μL each) were added to sterile Whatman filter disks and allowed to dry in a fume hood before discs were placed onto swarm agar surfaces. Plates were incubated upright at 30°C for 24 h. The diameters of the zones of clearing or haze were measured, and the diameter of the disk (6 mm) was subtracted from all measurements to yield the reported values. The total amount of antibiotic or detergent added to each disk is as follows: kanamycin (100 μg), rifampicin (100 μg), vancomycin (1 mg), CHIR-090 (100 μg, APExBIO), bacitracin (50 μg), TWEEN 20 (10 μL of 10% solution), Triton X-100 (10 μL of 10% solution), sodium dodecyl sulfate (10 μL of 10% solution). Tests using CHIR-090 used one-quarter of the standard amount of cells to reduce growth haze. For strains overexpressing genes integrated at the *vanA* locus, uninduced cells were grown in PYE/kanamycin or PYE/gentamicin, and aliquots were plated in PYE swarm agar on PYE medium. Induced cells were grown in PYE/kanamycin or PYE/gentamicin containing 0.5 mM vanillate before plating in/on PYE medium containing 0.5 mM vanillate. 100 μM 2,2′-dipyridyl was included in media for testing chemical sensitivity in iron-restricted conditions.

**Streptonigrin sensitivity—**Isolated colonies of the indicated strains were grown in PYE medium to $OD_{660}$ = 0.2–0.5 and diluted to $OD_{660}$ = 0.01. The diluted culture was aliquoted into separate tubes, which received 0.025 μg/mL, 0.25 μg/mL, or no streptonigrin (SNG). After 24 h of growth at 30°C, $OD_{660}$ values were measured, and optical density ratios (0.25 μg/mL SNG/no addition and 0.025 μg/mL SNG/no addition) were calculated as a measure of growth inhibition.

**Limulus amebocyte lysate assay—**The ToxinSensor Chromogenic LAL Endotoxin Assay kit (GenScript) was used to determine endotoxin units/mL of culture. Cells were grown to mid-exponential phase ($OD_{660}$ 0.2–0.5), washed twice with non-pyrogenic LAL reagent water, and normalized in this water to $OD_{660}$ = 0.1. Cell suspensions were serially diluted in non-pyrogenic water and analyzed according to manufacturer's instructions.

**Gel electrophoresis of lipid A species—**For visualizing LPS species from whole-cell lysates, cells were harvested after overnight growth in the indicated medium. All cultures were normalized by $OD_{660}$, pelleted, and resuspended to 100 μL in 1× tricine loading buffer (100 mM Tris-HCl pH 6.8, 1% sodium dodecyl sulfate (SDS), 20% glycerol, 0.02% Coomassie G-250, 1% 2-mercaptoethanol). Proteinase K (125 ng/μL final concentration) was added, and samples were incubated overnight at 55°C. Lysates were boiled 5 min, and equal volumes (10% of each sample) were analyzed by gel electrophoresis.

Hot aqueous-phenol LPS extractions were adapted from Westpahl and Jann (Davis and Goldberg, 2012; Westphal and Jann, 1965). 1 mL of culture at $OD_{660}$ = 0.75 was pelleted and resuspended in 200 μL 1× tricine loading buffer. Suspensions were boiled for 15 min and cooled to room temperature. 5 μL of 20 mg/mL Proteinase K was added to each sample before incubation at 55°C for three hours. Suspensions were mixed with 200 μL ice-cold Tris-saturated phenol, vortexed, and incubated at 65°C for 15 min before being cooled

to room temperature. 1 mL diethyl ether was added to each sample before vortexing and spinning for 10 min in a table-top centrifuge at 16,000 × *g*. The bottom blue layer was removed to a fresh tube, and the extraction was repeated on the blue layer starting from the phenol step. 200 μL 2× tricine loading buffer was added to each sample before gel electrophoresis.

Rough LPS was extracted by the method of Darveau and Hancock (Darveau and Hancock, 1983), modified as described (Hershey et al., 2019), beginning with 50 mL PYE cultures grown to $OD_{660}$ = 0.85. Cultures were centrifuged, and cell pellets were resuspended in 2 mL 10 mM Tris-HCl (pH 8.0) containing 2 mM $MgCl_2$. Samples were sonicated (Qsonica Q500) on ice for 5 min at 20% amplitude, in cycles of 10 s on/20 s off so that fewer than 5% of cells remained intact. DNase I and RNase A were added to final concentrations of 100 μg/mL and 25 μg/mL, respectively, and lysates were incubated at 37°C for 1 h. Additional DNase I and RNase A were added to reach final concentrations of 200 μg/mL and 50 μg/mL, respectively, and lysates were incubated for 1 h at 37°C. SDS and EDTA were added to achieve final concentrations of 2% and 100 mM, respectively, and lysates were incubated for 2 h at 37°C before centrifugation (30 min at 50,000 × *g*, 30 min, 4°C). Proteinase K (50 μg/mL) was added to each supernatant, followed by incubation for 2 h at 60°C. LPS was precipitated by the addition of 2 volumes of ice-cold 0.375 M $MgCl_2$/95% ethanol and collected by centrifugation (12,000 × *g*, 15 min, 4°C). Precipitates were resuspended in 3.3 mL 10 mM Tris-HCl (pH 8.0)/2% SDS/100 mM EDTA and incubated with shaking overnight at 37°C. Rough LPS was reprecipitated using 2 volumes ice-cold 0.375 M $MgCl_2$/95% ethanol and collected by centrifugation (12,000 × *g*, 15 min, 4°C). Precipitates were suspended in 10 mL10 mM Tris-HCl (pH 8.0) and centrifuged (200,000 × *g*, 2 h, 4°C). After removal of the supernatant by pipetting, LPS pellets were resuspended in 1 mL 1× tricine loading buffer, and 5 μL were analyzed by gel electrophoresis.

Free lipid A was extracted by the Caroff method (El Hamidi et al., 2005), modified as described (Leung et al., 2017), starting with 10 mL of PYE culture grown to $OD_{600}$ = 0.6. Cultures were divided into multiple tubes and centrifuged at 14,000 × *g* for 2 min. In a fume hood, cell pellets from each culture were resuspended, combined, and transferred to a gasketed microcentrifuge tube using 250 μL 70% (v/v) isobutyric acid +150 μL 1 M ammonium hydroxide. Samples were incubated in a boiling water bath in a fume hood for 1 h, with vortexing every 15 min. Samples were cooled on ice and centrifuged at 2000 × *g* for 15 min. In a fume hood, supernatants (~400 μL) were transferred to new gasketed tubes, each containing 400 μL endotoxin-free water. Small holes were punched in the gasketed caps using a syringe needle before the samples were frozen in liquid nitrogen and lyophilized overnight. Methanol (1 mL) was added, and samples were sonicated in a water bath for 5 min. Samples were centrifuged at 10,000 × *g* for 5 min, and methanol was aspirated. The methanol wash was repeated before lipids were solubilized in 190 μL 3:1.5:0.25 v/v/v chloroform:methanol:endotoxin-free water. After vortexing, samples were centrifuged at 8,000 × *g* for 5 min. Supernatants were transferred to fresh gasketed tubes, and extracts were dried under a stream of nitrogen before analysis by mass spectrometry (see below) or gel electrophoresis. Samples for gel electrophoresis were resuspended using 100 μL 1× tricine loading buffer, and 10 μL of each sample was analyzed.

All lipid samples were analyzed on 16.5% Mini-PROTEAN Tris-Tricine gels (Bio-Rad). Carbohydrates were stained using Pro-Q Emerald 300 Lipopolysaccharide Gel Stain Kit (Molecular Probes; P20495) per manufacturer's instructions. For Western blot analysis of S-LPS, equal numbers of cells grown in PYE with appropriate additions were pelleted, resuspended in 1× SDS loading buffer, and boiled before analysis on 12% polyacrylamide gels and transfer to Immobilon-P PVDF membranes. Blots were probed with α-S-LPS (1:20,000) (Walker et al., 1994) and horseradish peroxidase-conjugated anti-rabbit antibodies (1:5000) and analyzed using Western Lightning (PerkinElmer). Stained lipid species were visualized using a Bio-Rad Gel Doc XR.

**High performance liquid chromatography-tandem mass spectrometry (HPLC-MSMS) of lipid A extracts—**All samples for HPLC-electrospray ionization tandem mass spectrometry were generated by the modified Caroff extraction protocol described above. Each extract was initially dissolved in 100 μL 1:2 chloroform: methanol before dilution 1:10 with methanol for analysis. A 2–5 μL aliquot of each solution was injected onto a Phenomenex Jupiter C4 column (2 × 50 mm, 5 μm, 300 Å) for HPLC-MSMS analysis with a Waters Acquity UPLC system coupled to a Thermo LTQ-Orbitrap Velos Pro mass spectrometer, which was equipped with an atmospheric pressure electrospray ionization source. For lipid detection, the HPLC-MSMS analyses were carried out with full-mass detection over a mass range of *m/z* 250 to 2000 in the Fourier transform MS mode, with negative-ion detection. The mass resolution was 60,000 FWHM @ *m/z* 400. Fragmentation product ion masses of the three most intense precursor ions were measured in the ion trap or orbitrap (7500 resolution) mass analyzer using stepped collision-induced dissociation (35% of the normalized collision energy) or higher energy collision-induced dissociation (35% of the normalized collision energy) activation energies. During data acquisitions, real-time mass calibration was applied with *m/z* 283.26454 as the lock mass for negative-ion detection. The mobile phase for separation was (A) 1 mM ammonium acetate solution and (B) 90% (1:1 acetonitrile/propanol)/10% water/1 mM ammonium acetate as the binary solvents for the 16-min gradient elution: 0 to 10 min, 30% to 100%B; 10 to 12 min, 100% B and 12 to 12.1 min at 30% B, followed by column equilibration at 30% B from 12.1 to 16 min. The column flow rate was 0.35 mL/min and the column temperature was maintained at 40°C.

**Lipid A structure analysis—**MALDI-TOF MS was used to screen lipid extracts. To check structures, tandem MS and ancillary separation techniques were required. These are described below. HPLC-MSMS (above) describes the generation of data for structure determinations in Figure S3. Notably, the triple deletion strain Δ*ctpA* Δ*fur* Δ*sspB* contained no lipid A with sugars at the terminal (1 and 4′) positions but rather contained phosphates, as found in canonical lipid A structures. The Δ*lpxC* Δ*fur* Δ*sspB* strain contained an ion at 1412 *m/z*, the structure of which remains unclear. The HPLC-MSMS data of this ion showed no loss of phosphate, as seen in Δ*ctpA* Δ*fur* Δ*sspB*, nor loss of sugars, as seen for the NA1000, Δ*sspB*, or Δ*fur* Δ*sspB* strains. The fragmentation pattern strongly suggested that something other than lipid A was responsible for the ion at 1412 *m/z*. Given that cardiolipin is a common microbial membrane lipid, we carried out HILIC-MS (described below) with cardiolipin and lipid A standards. Both standards were retained by HILIC,

as expected for hydrophobic molecules, but extracts from the Δ*lpxC* Δ*fur* Δ*sspB* mutant showed no ions at all, suggesting that the species at 1412 *m/z* is not hydrophobic enough to be retained. Regrettably, there remains no structure identified for the ion at 1412 *m/z*. Generally, structure analysis was conducted manually according to our prior effort in this field (Yoon et al., 2016).

**Hydrophobic interaction liquid chromatography-mass spectrometry (HILIC-MS)—**A 10-μL aliquot of each solution was injected into a Waters Atlantis HILIC column (4.6 mm × 150 mm, 5 μm) to run LC-MS on a Water Acquity UPLC system coupled to a Thermo LTQ-Orbitrap Velos Pro mass spectrometer, which was equipped with an atmospheric pressure electrospray ionization source. For lipid detection, the HILIC-MS runs were carried out with full-mass detection over a mass range of *m/z* 80 to 2000 in the Fourier transform MS mode, with positive-ion and negative-ion detection, respectively, in two rounds of LC injections. The mass resolution was 60,000 FWHM @ *m/z* 400. During data acquisitions, real-time mass calibration was applied with *m/z* 391.28426 as the lock mass for positive-ion detection and with *m/z* 112.98563 as the lock mass for negative-ion detection. The mobile phase of HILIC was (A) 20 mM ammonium acetate solution (pH adjusted to 4.0 with acetic acid) and (B) methanol as the binary solvents for gradient elution: 0–4 min, 99% B; 4 to 12.5 min, 99%–20% B and 12.5 to 15 min at 20% B, followed by column equilibration at 99% B for 5 min between injections. The column flow rate was 0.4 mL/min and the column temperature was maintained at 40°C.

**Microscopy—**Cells were immobilized on agarose pads (1% w/v in reverse osmosis-purified water). Images were taken using a Zeiss EC Plan-Neofluar 100×/1.3 Oil M27 objective on a Zeiss AxioImager M1 microscope with a Hamamatsu Digital CCD Camera (C8484-03G01). Images were acquired using iVision-Mac software (BioVision Technologies) and processed using ImageJ (Rasband, W.S., ImageJ, U. S. National Institutes of Health, Bethesda, Maryland, USA, https://imagej.nih.gov/ij/, 1997–2018).

**CryoEM imaging—**Cultures (5 mL) of KR4000, KR4102, KR4103, and KR3906 grown to $OD_{660}$ 0.2–0.5 were centrifuged (4°C, 16,000 × *g*, 15 min), and cell pellets were resuspended in 50 μL PYE. For KR3906, cells grown in PYEX were washed twice with PYE, released into PYED at $OD_{660}$ = 0.02, and incubated for 12 h before harvest. 3 μL of cell suspension, mixed 1:1 with fiducial markers (10-nm gold particles conjugated to Protein A; Aurion) was applied to glow-discharged quantifoil grids (R2/2) and frozen in liquid ethane using an automatic plunge freezing device (Vitrobot, FEI. 12°C, 8–12s blot time, blot force 8, humidity 100%).

Grids of KR4000 and KR4103 were imaged on a Jeol3100 cryoTEM operating at 300kV with in column omega energy filter and K2 direct electron camera. Grids of KR4102 and KR3906 were imaged on a Krios Cryo TEM (FEI) operating at 300kV with post column energy filter (Quantum, GATAN) and K2 direct electron camera. All data were collected with the automatic data collection program serialEM (Mastonarde, 2005). Square overview images were acquired using a defocus of 80–100 microns at a nominal magnification of 3600–6500× (Krios) or 1200× (Jeol) using the polygon montage operation (specimen pixel size: 33–67Å). Beam intensity was set to $8e^{-}$/px/s over an empty hole and exposure times

ranged from 2 to 5s depending on ice thickness. Bidirectional tomographic tilt series were collected from ±60° using a defocus of 6–8 μm and at a magnification which provided specimen pixel size of 4–7 Å. Total dose of the tilt series were kept between 60 and 90 $e^{-}/Å^{2}$. All tilt series images were collected in movie mode and the frames aligned using MotionCor2 (Zheng et al., 2017). Aligned frames were compiled into stacks and processed using IMOD (Kremer et al., 1996). Contrast of resulting tomograms was enhanced using a non-linear anisotropic diffusion filter (Frangakis and Hegerl, 2001) and manually segmented using the 3D visualization program AMIRA (ThermoFisher).

**RB-Tnseq analysis—**A 1 mL aliquot of the RB-Tnseq library in NA1000 (Price et al., 2018) was thawed and grown to $OD_{660}$ = 0.65 in 25 mL PYE medium with kanamycin. Aliquots of this culture were saved for sequencing of pre-challenge barcodes, or were diluted to $OD_{660}$ = 0.02 in PYE medium (set8IT011, set8IT023, and set8IT035) or PYE medium with 2 μg/mL CHIR-090 (set8IT012, set8IT024, and set8IT036). Cultures were grown for 9 h at 30°C as described (Price et al., 2018) before cells were harvested and post-challenge barcodes were sequenced. Gene fitness (f) and significance (t) scores were calculated as described (Wetmore et al., 2015). Candidate genes examined in this study (*CCNA_01217-01220*) had fitness scores between −1.5 and −3.7, with signficance scores between −3.0 and −8.4, for individual trials of library growth in PYE + CHIR-090.

**Sphingolipid extraction and liquid chromatography-tandem mass spectrometry (LC-MS/MS)—***Caulobacter* strains were grown overnight with or without 0.5 mM vanillate (5 mL), and lipids were extracted by the method of Bligh and Dyer (Bligh and Dyer, 1959). Cells were harvested and resuspended in 1 mL of water, 3.75 mL of 1:2 (v/v) chloroform: methanol was added, and the samples were mixed by vortexing. Chloroform (1.25 mL) and water (1.25 mL) were added sequentially with vortexing to create a two-phase system and the samples were centrifuged at 200 × *g* for 5 min at room temperature. The bottom, organic phase was transferred to a clean glass tube with a Pasteur pipette and washed twice in “authentic” upper phase. Subsequently, the organic phase containing lipids was collected and dried under argon. Our methods for lipid analysis by normal phase LC/ESI–MS/MS have been described (Guan et al., 2014). Briefly, normal phase LC was performed on an Agilent 1200 Quaternary LC system equipped with an Ascentis Silica HPLC column, 5 μm, 25 cm × 2.1 mm (Sigma-Aldrich, St. Louis, MO) as described. The LC eluent (with a total flow rate of 300 μL/min) was introduced into the ESI source of a high resolution TripleTOF5600 mass spectrometer (Applied Biosystems, Foster City, CA). Instrumental settings for negative ion ESI and MS/MS analysis of lipid species were as follows: ion spray voltage (IS) = −4500 V; curtain gas (CUR) = 20 psi; ion source gas 1 (GSI) = 20 psi; declustering potential (DP) = −55 V; and focusing potential (FP) = −150 V. The MS/MS analysis used nitrogen as the collision gas. Data analysis was performed using Analyst TF1.5 software (Applied Biosystems, Foster City, CA).

## QUANTIFICATION AND STATISTICAL ANALYSIS

Except for RB-TnSeq analysis, all quantitative data were shown as the mean ± S.D. for the number of biological replicates stated in the figure legend or graphed as individual values. GraphPad Prism 9.3.1 was used to perform the tests of statistical significance described in

figure legends. The following symbols were used for all significance tests: ****, $p < 0.0001$; ***, $0.0001 < p < 0.001$; **, $0.001, p < 0.01$; *, $0.01 < p < 0.05$; n.s., not significant $p > 0.05$.

For RB-Tnseq data, the average gene fitness scores graphed in Figure 5A represent the means of three control experiments (PYE, x-axis) and three challenges of the library with 2 μg/mL CHIR-090 (y-axis). Gene fitness is the weighted average of strain fitness, across strains that have a transposon inserted within that gene. A strain's fitness is the $\log_2$ ratio of abundance at the end of the experiment compared with its abundance at the beginning of the experiment, where the number of reads of each strain's unique barcode is a proxy for its abundance. For each gene in each experiment, a *t*-like statistic is calculated that indicates how reliably the fitness score is different from zero (indicating a neutral effect). All raw data are available at https://fit.genomics.lbl.gov, and statistical analyses are described in detail in a methods paper (Wetmore et al., 2015).

## Supplementary Material

Refer to Web version on PubMed Central for supplementary material.

## ACKNOWLEDGMENTS

The authors thank Charlie Huang, Morgan Price, Laura Herron, and Henry Seaborne for experimental assistance. Cryoelectron microscopy data acquisition was performed using instrumentation of Lawrence Berkeley National Laboratory and the Bay Area CryoEM resource, maintained by Jonathan Remis, Daniel Toso, and Paul Tobias. D.R.G. thanks the International Centre for Cancer Vaccine Science project of the International Research Agendas program of the Foundation for Polish Science, co-financed by the European Union under the European Regional Development Fund MAB/2017/03 at the University of Gdansk. Funding for this work was provided by National Science Foundation awards 1553004 and 2031948 (to E.A.K.) and 1615287 (to K.R.R.) and National Institutes of Health awards GM111066-01 and 1R01AI123820-01 (to D.R.G.). Cryoelectron tomography work was supported by the Laboratory Directed Research and Development Program of Lawrence Berkeley National Laboratory under U.S. Department of Energy contract DE-AC02-05CH11231.

## REFERENCES

Afgan E, Baker D, van den Beek M, Blankenberg D, Bouvier D, Cech M, Chilton J, Clements D, Coraor N, Eberhard C, et al. (2016). The Galaxy platform for accessible, reproducible and collaborative biomedical analyses: 2016 update. Nucleic Acids Res. 44, W3–W10. 10.1093/nar/gkw343. [PubMed: 27137889]

Altschul S (1997). Gapped BLAST and PSI-BLAST: a new generation of protein database search programs. Nucleic Acids Res. 25, 3389–3402. 10.1093/nar/25.17.3389. [PubMed: 9254694]

Altschul SF, Gish W, Miller W, Myers EW, and Lipman DJ (1990). Basic local alignment search tool. J. Mol. Biol. 215, 403–410. 10.1016/S0022-2836(05)80360-2. [PubMed: 2231712]

Andrews S, Norton I, Salunkhe AS, Goodluck H, Aly WSM, Mourad-Agha H, and Cornelis P (2013). Control of iron metabolism in bacteria. Met. Ions Life Sci. 12, 203–239. 10.1007/978-94-007-5561-1_7. [PubMed: 23595674]

Awram P, and Smit J (2001). Identification of lipopolysaccharide O antigen synthesis genes required for attachment of the S-layer of *Caulobacter crescentus*. Microbiology 147, 1451–1460. 10.1099/00221287-147-6-1451. [PubMed: 11390676]

Bligh EG, and Dyer WJ (1959). A rapid method of total lipid extraction and purification. Can J. Biochem. Physiol. 37, 911–917. 10.1139/o59-099. [PubMed: 13671378]

Blondelet-Rouault MH, Weiser J, Lebrihi A, Branny P, and Pernodet JL (1997). Antibiotic resistance gene cassettes derived from the omega interposon for use in *E. coli* and *Streptomyces*. Gene 190, 315–317. 10.1016/s0378-1119(97)00014-0. [PubMed: 9197550]

Boll JM, Crofts AA, Peters K, Cattoir V, Vollmer W, Davies BW, and Trent MS (2016). A penicillin-binding protein inhibits selection of colistin-resistant, lipooligosaccharide-deficient *Acinetobacter baumannii*. Proc. Natl. Acad. Sci. USA 113, E6228–E6237. 10.1073/pnas.1611594113. [PubMed: 27681618]

Brown DB, Forsberg LS, Kannenberg EL, and Carlson RW (2012). Characterization of galacturonosyl transferase genes *rgtA, rgtB, rgtC, rgtD*, and *rgtE* responsible for lipopolysaccharide synthesis in nitrogen-fixing endosymbiont *Rhizobium leguminosarum*: lipopolysaccharide core and lipid galacturonosyl residues confer membrane stability. J. Biol. Chem. 287, 935–949. 10.1074/jbc.m111.311571. [PubMed: 22110131]

Brown DB, Muszynski A, and Carlson RW (2013). Elucidation of a novel lipid A alpha-(1,1)-GalA transferase gene (rgtF) from Mesorhizobium loti: heterologous expression of rgtF causes Rhizobium etli to synthesize lipid A with alpha-(1,1)-GalA. Glycobiology 23, 546–558. 10.1093/glycob/cws223. [PubMed: 23283001]

Chien P, Perchuk BS, Laub MT, Sauer RT, and Baker TA (2007). Direct and adaptor-mediated substrate recognition by an essential AAA+ protease. Proc. Natl. Acad. Sci. USA 104, 6590–6595. 10.1073/pnas.0701776104. [PubMed: 17420450]

Christen B, Abeliuk E, Collier JM, Kalogeraki VS, Passarelli B, Coller JA, Fero MJ, McAdams HH, and Shapiro L (2011). The essential genome of a bacterium. Mol. Syst. Biol. 7, 528. 10.1038/msb.2011.58. [PubMed: 21878915]

Crosson S, McGrath PT, Stephens C, McAdams HH, and Shapiro L (2005). Conserved modular design of an oxygen sensory/signaling network with species-specific output. Proc. Natl. Acad. Sci. USA 102, 8018–8023. 10.1073/pnas.0503022102. [PubMed: 15911751]

da Silva Neto JF, Braz VS, Italiani VCS, and Marques MV (2009). Fur controls iron homeostasis and oxidative stress defense in the oligotrophic alpha-proteobacterium *Caulobacter crescentus*. Nucleic Acids Res. 37, 4812–4825. 10.1093/nar/gkp509. [PubMed: 19520766]

da Silva Neto JF, Lourenco RF, and Marques MV (2013). Global transcriptional response of *Caulobacter crescentus* to iron availability. BMC Genomics 14, 549. 10.1186/1471-2164-14-549. [PubMed: 23941329]

Darveau RP, and Hancock RE (1983). Procedure for isolation of bacterial lipopolysaccharides from both smooth and rough *Pseudomonas aeruginosa* and *Salmonella typhimurium* strains. J. Bacteriol. 155, 831–838. 10.1128/jb.155.2.831-838.1983. [PubMed: 6409884]

Davis MR Jr, and Goldberg JB (2012). Purification and visualization of lipopolysaccharide from Gram-negative bacteria by hot aqueous-phenol extraction. J. Vis. Exp. 28, e3916. 10.3791/3916.

De Castro C, Molinaro A, Lanzetta R, Silipo A, and Parrilli M (2008). Lipopolysaccharide structures from *Agrobacterium* and *Rhizobiaceae* species. Carbohydr. Res. 343, 1924–1933. 10.1016/j.carres.2008.01.036. [PubMed: 18353297]

Dehio C, and Meyer M (1997). Maintenance of broad-host-range incompatibility group P and group Q plasmids and transposition of Tn5 in *Bartonella henselae* following conjugal plasmid transfer from *Escherichia coli*. J. Bacteriol. 179, 538–540. 10.1128/jb.179.2.538-540.1997. [PubMed: 8990308]

El Hamidi A, Tirsoaga A, Novikov A, Hussein A, and Caroff M (2005). Microextraction of bacterial lipid A: easy and rapid method for mass spectrometric characterization. J. Lipid Res. 46, 1773–1778. 10.1194/jlr.d500014-jlr200. [PubMed: 15930524]

Ely B (1991). Genetics of *Caulobacter crescentus*. Methods Enzymol. 204, 372–384. 10.1016/0076-6879(91)04019-k. [PubMed: 1658564]

Evinger M, and Agabian N (1977). Envelope-associated nucleoid from *Caulobacter crescentus* stalked and swarmer cells. J.Bacteriol. 132, 294–301. 10.1128/jb.132.1.294-301.1977. [PubMed: 334726]

Fontenot CR, Tasnim H, Valdes KA, Popescu CV, and Ding H (2020). Ferric uptake regulator (Fur) reversibly binds a [2Fe-2S] cluster to sense intracellular iron homeostasis in *Escherichia coli*. J. Biol. Chem. 295, 15454–15463. 10.1074/jbc.ra120.014814. [PubMed: 32928958]

Frangakis AS, and Hegerl R (2001). Noise reduction in electron tomographic reconstructions using nonlinear anisotropic diffusion. J. Struct. Biol. 135, 239–250. 10.1006/jsbi.2001.4406. [PubMed: 11722164]

Garrison E, and Marth G (2012). Haplotype-based variant detection from short-read sequencing. Preprint at arXiv. 10.48550/ARXIV.1207.3907.

Gilchrist A, and Smit J (1991). Transformation of freshwater and marine caulobacters by electroporation. J. Bacteriol. 173, 921–925. 10.1128/jb.173.2.921-925.1991. [PubMed: 1987172]

Guan Z, Katzianer D, Zhu J, and Goldfine H (2014). *Clostridium difficile* contains plasmalogen species of phospholipids and glycolipids. Biochim. Biophys. Acta 1842, 1353–1359. 10.1016/j.bbalip.2014.06.011. [PubMed: 24983203]

Hassett DJ, Britigan BE, Svendsen T, Rosen GM, and Cohen MS (1987). Bacteria form intracellular free radicals in response to paraquat and streptonigrin. Demonstration of the potency of hydroxyl radical. J. Biol. Chem. 262, 13404–13408. 10.1016/s0021-9258(19)76440-0. [PubMed: 2820968]

Henry R, Crane B, Powell D, Deveson Lucas D, Li Z, Aranda J, Harrison P, Nation RL, Adler B, Harper M, et al. (2015). The transcriptomic response of *Acinetobacter baumannii* to colistin and diripenem alone and in combination in an in vitro pharmacokinetics/pharmacodynamics model. J. Antimicrob. Chermother. 70, 1303–1313. 10.1093/jac/dku536.

Hershey DM, Fiebig A, and Crosson S (2019). A genome-wide analysis of adhesion in Caulobacter crescentus identifies new regulatory and biosynthetic components for holdfast assembly. mBio 10, 2273. 10.1128/mbio.02273-18.

Jones MD, Vinogradov E, Nomellini JF, and Smit J (2015). The core and O-polysaccharide structure of the *Caulobacter crescentus* lipopolysaccharide. Carbohydr. Res. 402, 111–117. 10.1016/j.carres.2014.10.003. [PubMed: 25498010]

Justino MC, Almeida CC, Teixeira M, and Saraiva LM (2007). *Escherichia coli* di-iron YtfE protein is necessary for the repair of stress-damaged iron-sulfur clusters. J. Biol. Chem. 282, 10352–10359. 10.1074/jbc.m610656200. [PubMed: 17289666]

Karbarz MJ, Kalb SR, Cotter RJ, and Raetz CRH (2003). Expression cloning and biochemical characterization of a *Rhizobium leguminosarum* lipid A 1-phosphatase. J. Biol. Chem. 278, 39269–39279. 10.1074/jbc.m305830200. [PubMed: 12869541]

Kawahara K, Seydel U, Matsuura M, Danbara H, Rietschel ET, and Zahringer U (1991). Chemical structure of glycosphingolipids isolated from *Sphingomonas paucimobilis*. FEBS Lett. 292, 107–110. 10.1016/0014-5793(91)80845-t. [PubMed: 1959589]

Kawasaki S, Moriguchi R, Sekiya K, Nakai T, Ono E, Kume K, and Kawahara K (1994). The cell envelope structure of the lipopolysaccharide-lacking Gram-negative bacterium *Sphingomonas paucimobilis*. J. Bacteriol. 176, 284–290. 10.1128/jb.176.2.284-290.1994. [PubMed: 8288520]

Keiler KC, Waller PR, and Sauer RT (1996). Role of a peptide tagging system in degradation of proteins synthesized from damaged messenger RNA. Science 271, 990–993. [PubMed: 8584937]

Kremer JR, Mastronarde DN, and McIntosh JR (1996). Computer visualization of three-dimensional image data using IMOD. J. Struct. Biol. 116, 71–76. 10.1006/jsbi.1996.0013. [PubMed: 8742726]

Langmead B, and Salzberg SL (2012). Fast gapped-read alignment with Bowtie 2. Nat. Methods 9, 357–359. 10.1038/nmeth.1923. [PubMed: 22388286]

Leaden L, Silva LG, Ribeiro RA, dos Santos NM, Lorenzetti APR, Alegria TGP, Schulz ML, Medeiros MHG, Koide T, and Marques MV (2018). Iron deficiency generates oxidative stress and activation of the SOS response in *Caulobacter crescentus*. Front. Microbiol. 9, 2014. 10.3389/fmicb.2018.02014. [PubMed: 30210482]

Leung LM, Fondrie WE, Doi Y, Johnson JK, Strickland DK, Ernst RK, and Goodlett DR (2017). Identification of the ESKAPE pathogens by mass spectrometric analysis of microbial membrane glycolipids. Sci. Rep. 7, 6403. 10.1038/s41598-017-04793-4. [PubMed: 28743946]

Levchenko I, Seidel M, Sauer RT, and Baker TA (2000). A specificity-enhancing factor for the ClpXP degradation machine. Science 289, 2354–2356. 10.1126/science.289.5488.2354. [PubMed: 11009422]

Liu L, Feng X, Wang W, Chen Y, Chen Z, and Gao H (2020). Free rather than total iron content is critically linked to the Fur physiology in *Shewanella oneidensis*. Front. Microbiol. 11, 593246. 10.3389/fmicb.2020.593246. [PubMed: 33329474]

Livak KJ, and Schmittgen TD (2001). Analysis of relative gene expression data using real-time quantitative PCR and the 2−ΔΔCT method. Methods 25, 402–408. 10.1006/meth.2001.1262. [PubMed: 11846609]

MacNair CR, Stokes JM, Carfrae LA, Fiebig-Comyn AA, Coombes BK, Mulvey MR, and Brown ED (2018). Overcoming *mcr-1* mediated colistin resistance with colistin in combination with other antibiotics. Nat. Commun. 9. 10.1038/s41467-018-02875-z.

Mamat U, Meredith TC, Aggarwal P, Kuhl A, Kirchhoff P, Lindner B, Hanuszkiewicz A, Sun J, Holst O, and Woodard RW (2008). Single amino acid substitutions in either YhjD or MsbA confer viability to 3-deoxy-D-mannooct-2-ulosonic acid-depleted *Escherichia coli*. Mol. Microbiol. 67, 633–648. 10.1111/j.1365-2958.2007.06074.x. [PubMed: 18093093]

Marks ME, Castro-Rojas CM, Teiling C, Du L, Kapatral V, Walunas TL, and Crosson S (2010). The genetic basis of laboratory adaptation in *Caulobacter crescentus*. J. Bacteriol. 192, 3678–3688. 10.1128/jb.00255-10. [PubMed: 20472802]

Martin M (2011). Cutadapt removes adapter sequences from high-throughput sequencing reads. EMBnet J. 17, 10. 10.14806/ej.17.1.200.

Mastronarde DN (2005). Automated electron microscope tomography using robust prediction of specimen movements. J. Struct. Biol. 152, 36–51. 10.1016/j.jsb.2005.07.007. [PubMed: 16182563]

McClerren AL, Endsley S, Bowman JL, Andersen NH, Guan Z, Rudolph J, and Raetz CRH (2005). A slow, tight-binding inhibitor of the zinc-dependent deacetylase LpxC of lipid A biosynthesis with antibiotic activity comparable to ciprofloxacin. Biochemistry 44, 16574–16583. 10.1021/bi0518186. [PubMed: 16342948]

Meisenzahl AC, Shapiro L, and Jenal U (1997). Isolation and characterization of a xylose-dependent promoter from *Caulobacter crescentus*. J. Bacteriol. 179, 592–600. 10.1128/jb.179.3.592-600.1997. [PubMed: 9006009]

Meredith TC, Aggarwal P, Mamat U, Lindner B, and Woodard RW (2006). Redefining the requisite lipopolysaccharide structure in *Escherichia coli*. ACS Chem. Biol. 1, 33–42. 10.1021/cb0500015. [PubMed: 17163638]

Moffatt JH, Harper M, and Boyce JD (2019). Mechanisms of polymyxin resistance. Adv. Exp. Med. Biol. 1145, 55–71. 10.1007/978-3-030-16373-0_5. [PubMed: 31364071]

Moffatt JH, Harper M, Harrison P, Hale JDF, Vinogradov E, Seemann T, Henry R, Crane B, St Michael F, Cox AD, et al. (2010). Colistin resistance in *Acinetobacter baumannii* is mediated by complete loss of lipopolysaccharide production. Antimicrob. Agents Chemother. 54, 4971–4977. 10.1128/aac.00834-10. [PubMed: 20855724]

Nachin L, El Hassouni M, Loiseau L, Expert D, and Barras F (2001). SoxR-dependent response to oxidative stress and virulence of *Erwinia chrysanthemi*: the key role of SufC, an orphan ABC ATPase. Mol. Microbiol. 39, 960–972. 10.1046/j.1365-2958.2001.02288.x. [PubMed: 11251816]

Nagiec MM, Skrzypek M, Nagiec EE, Lester RL, and Dickson RC (1998). The LCB4 (YOR171c) and LCB5 (YLR260w) genes of *Saccharomyces* encode sphingoid long chain base kinases. J. Biol. Chem. 273, 19437–19442. 10.1074/jbc.273.31.19437. [PubMed: 9677363]

Nagy E, Losick R, and Kahne D (2019). Robust suppression of lipopolysaccharide deficiency in *Acinetobacter baumannii* by growth in minimal medium. J. Bacteriol. 201, 420. 10.1128/jb.00420-19.

Nikaido H (2003). Molecular basis of bacterial outer membrane permeability revisited. Microbiol. Mol. Biol. Rev. 67, 593–656. 10.1128/mmbr.67.4.593-656.2003. [PubMed: 14665678]

Olea-Ozuna RJ, Poggio S, Bergström E, Quiroz-Rocha E, García-Soriano DA, Sahonero-Canavesi DX, Padilla-Gómez J, Martínez-Aguilar L, López-Lara IM, Thomas-Oates J, and Geiger O (2021). Five structural genes required for ceramide synthesis in *Caulobacter* and for bacterial survival. Environ. Microbiol. 23, 143–159. 10.1111/1462-2920.15280. [PubMed: 33063925]

Peng D, Hong W, Choudhury BP, Carlson RW, and Gu X-X (2005). *Moraxella cararrhalis* bacterium without endotoxin, a potential vaccine candidate. Infect. Immun. 73, 7569–7577. 10.1128/iai.73.11.7569-7577.2005. [PubMed: 16239560]

Plötz BM, Lindner B, Stetter KO, and Holst O (2000). Characterization of a novel lipid A containing D-galacturonic acid that replaces phosphate residues. The structure of the lipid a of the lipopolysaccharide from the hyperthermophilic bacterium *Aquifex pyrophilus*. J. Biol. Chem. 275, 11222–11228. 10.1074/jbc.275.15.11222. [PubMed: 10753930]

Price MN, Wetmore KM, Waters RJ, Callaghan M, Ray J, Liu H, Kuehl JV, Melnyk RA, Lamson JS, Suh Y, et al. (2018). Mutant phenotypes for thousands of bacterial genes of unknown function. Nature 557, 503–509. 10.1038/s41586-018-0124-0. [PubMed: 29769716]

Qureshi N, Takayama K, Mascagni P, Honovich J, Wong R, and Cotter RJ (1988). Complete structural determination of lipopolysaccharide obtained from deep rough mutant of *Escherichia coli*. Purification by high performance liquid chromatography and direct analysis by plasma desorption mass spectrometry. J. Biol. Chem. 263, 11971–11976. 10.1016/s0021-9258(18)37881-5. [PubMed: 3136169]

Radolf JD, and Kumar S (2018). The *Treponema pallidum* outer membrane. Curr. Top. Microbiol. Immuno. 415, 1–38. 10.1007/82_2017_44.

Rojas ER, Billings G, Odermatt PD, Auer g K., Zhu L, Miguel A, Chang F, Weibel DB, Theriot JA, and Huang KC (2018). The outer membrane is an essential load-bearing element in Gram-negative bacteria. Nature 559, 617–621. 10.1038/s41586-018-0344-3. [PubMed: 30022160]

Sabnis A, Hagart KLH, Klöckner A, Becce M, Evans LE, Furniss RCD, Mavridou DA, Murphy R, Stevens MM, Davies JC, Larrouy-Maumus GJ, Clarke TB, and Edwards AM (2021). Colistin kills bacteria by targeting lipopolysaccharide in the cytoplasmic membrane. eLife 10, e65836. 10.7554/eLife.65836. [PubMed: 33821795]

Samuel G, and Reeves P (2003). Biosynthesis of O-antigens: genes and pathways involved in nucleotide sugar precursor synthesis and O-antigen assembly. Carboyhdr. Res. 338, 2503–2519. 10.1016/j.carres.2003.07.009.

Shapland EB, Reisinger SJ, Bajwa AK, and Ryan KR (2011). An essential tyrosine phosphatase homolog regulates cell separation, outer membrane integrity, and morphology in *Caulobacter crescentus*. J. Bacteriol. 193, 4361–4370. 10.1128/jb.00185-11. [PubMed: 21705597]

Simpson BW, Nieckarz M, Pinedo V, McLean AB, Cava F, and Trent MS (2021). Acinetobacter baumannii can survive with an outer membrane lacking lipooligosaccharide due to structural support from elongasome peptidoglycan synthesis. mBio 12, e0309921. 10.1128/mbio.03099-21. [PubMed: 34844428]

Skerker JM, Prasol MS, Perchuk BS, Biondi EG, and Laub MT (2005). Two-component signal transduction pathways regulating growth and cell cycle progression in a bacterium: a system-level analysis. PLoS Biol. 3, e334. 10.1371/journal.pbio.0030334. [PubMed: 16176121]

Smit J, Kaltashov IA, Cotter RJ, Vinogradov E, Perry MB, Haider H, and Qureshi N (2008). Structure of a novel lipid A obtained from the lipopolysaccharide of *Caulobacter crescentus*. Innate Immun. 14, 25–36. 10.1177/1753425907087588. [PubMed: 18387917]

Stankeviciute G, Guan Z, Goldfine H, and Klein EA (2019). Caulobacter crescentus adapts to phosphate starvation by synthesizing anionic glycoglycerolipids and a novel glycosphingolipid. mBio 10, 107. 10.1128/mbio.00107-19.

Stankeviciute G, Tang P, Ashley B, Chamberlain JD, Hansen MEB, Coleman A, D'Emilia R, Fu L, Mohan EC, Nguyen H, et al. (2022). Convergent evolution of bacterial ceramide synthesis. Nat. Chem. Biol. 18, 305–312. 10.1038/s41589-021-00948-7. [PubMed: 34969973]

Steeghs L, den Hartog R, den Boer A, Roholl P, and van der Ley P (1998). Meningitis bacterium is viable without endotoxin. Nature 392, 449–450. 10.1038/33046. [PubMed: 9548250]

Thanbichler M, Iniesta AA, and Shapiro L (2007). A comprehensive set of plasmids for vanillate- and xylose-inducible gene expression in *Caulobacter crescentus*. Nucleic Acids Res. 35, e137. 10.1093/nar/gkm818. [PubMed: 17959646]

Toh E,, Kurtz, H.D., and Brun, Y.V. (2008). Characterization of the *Caulobacter crescentus* holdfast polysaccharide biosynthesis pathway reveals significant redundancy in the initiating glycosyltransferase and polyerase steps. J. Bacteriol. 190, 7219–7231. 10.1128/jb.01003-08. [PubMed: 18757530]

Velkov T, Thompson PE, Nation RL, and Li J (2010). Structure-activity relationships of polymyxin antibiotics. J. Med. Chem. 53, 1898–1916. 10.1021/jm900999h. [PubMed: 19874036]

Walker SG, Karunaratne DN, Ravenscroft N, and Smit J (1994). Characterization of mutants of *Caulobacter crescentus* defective in surface attachment of the paracrystalline surface layer. J. Bacteriol. 176, 6312–6323. 10.1128/jb.176.20.6312-6323.1994. [PubMed: 7929003]

Wang X, Ribeiro AA, Guan Z, McGrath SC, Cotter RJ, and Raetz CRH (2006). Structure and biosynthesis of free lipid A molecules that replace lipopolysaccharide in *Francisella tularensis* subsp. novicida. Biochemistry 45, 14427–14440. 10.1021/bi061767s. [PubMed: 17128982]

Westphal O, and Jann K (1965). Bacterial lipopolysaccharides extraction with phenol-water and further applications of the procedure. Methods Carbohydr. Chem. 5, 83–91.

Wetmore KM, Price MN, Waters RJ, Lamson JS, He J, Hoover CA, Blow MJ, Bristow J, Butland G, Arkin AP, and Deutschbauer A (2015). Rapid quantification of mutant fitness in diverse bacteria by sequencing randomly bar-coded transposons. mBio 6, e00306–e00315. 10.1128/mbio.00306-15. [PubMed: 25968644]

Whitfield C, and Trent MS (2014). Biosynthesis and export of bacterial lipopolysaccharides. Annu. Rev. Biochem. 83, 99–128. 10.1146/annurev-biochem-060713-035600. [PubMed: 24580642]

Wofford JD, Bolaji N, Dziuba N, Outten FW, and Lindahl PA (2019). Evidence that a respiratory shield in Escherichia coli protects a low-molecular-mass Fe(II) pool from $O_2$-dependent oxidation. J. Biol. Chem. 294, 50–62. 10.1074/jbc.ra118.005233. [PubMed: 30337367]

Yeowell HN, and White JR (1982). Iron requirement in the bactericidal mechanism of streptonigrin. Antimicrob. Agents Chemother. 22, 961–968. 10.1128/aac.22.6.961. [PubMed: 6218780]

Yoon SH, Liang T, Schneider T, Oyler BL, Chandler CE, Ernst RK, Yen GS, Huang Y, Nilsson E, and Goodlett DR (2016). Rapid lipid A structure determination via surface acoustic wave nebulization and hierarchical tandem mass spectrometry algorithm. Rapid Commun. Mass Spectrom. 30, 2555–2560. 10.1002/rcm.7728. [PubMed: 27582344]

Zhang G, Meredith TC, and Kahne D (2013). On the essentiality of lipopolysaccharide to Gram-negative bacteria. Curr. Opin. Microbiol. 16, 779–785. 10.1016/j.mib.2013.09.007. [PubMed: 24148302]

Zheng SQ, Palovcak E, Armache JP, Verba KA, Cheng Y, and Agard DA (2017). MotionCor2: anisotropic correction of beam-induced motion for improved cryo-electron microscopy. Nat. Methods 14, 331–332. 10.1038/nmeth.4193. [PubMed: 28250466]

Zhou B, Schrader JM, Kalogeraki VS, Abeliuk E, Dinh CB, Pham JQ, Cui ZZ, Dill DL, McAdams HH, and Shapiro L (2015). The global regulatory architecture of transcription during the *Caulobacter* cell cycle. Plos Genet. 11, e1004831. 10.1371/journal.pgen.1004831. [PubMed: 25569173]

## Highlights

- Lipid A is conditionally essential for viability in *Caulobacter crescentus*
- Inactivation of Fur is required for survival of lipid A-deficient *Caulobacter*
- Anionic sphingolipids promote *Caulobacter* fitness in the absence of lipid A
- Anionic sphingolipids, rather than LPS, underlie colistin sensitivity in *Caulobacter*

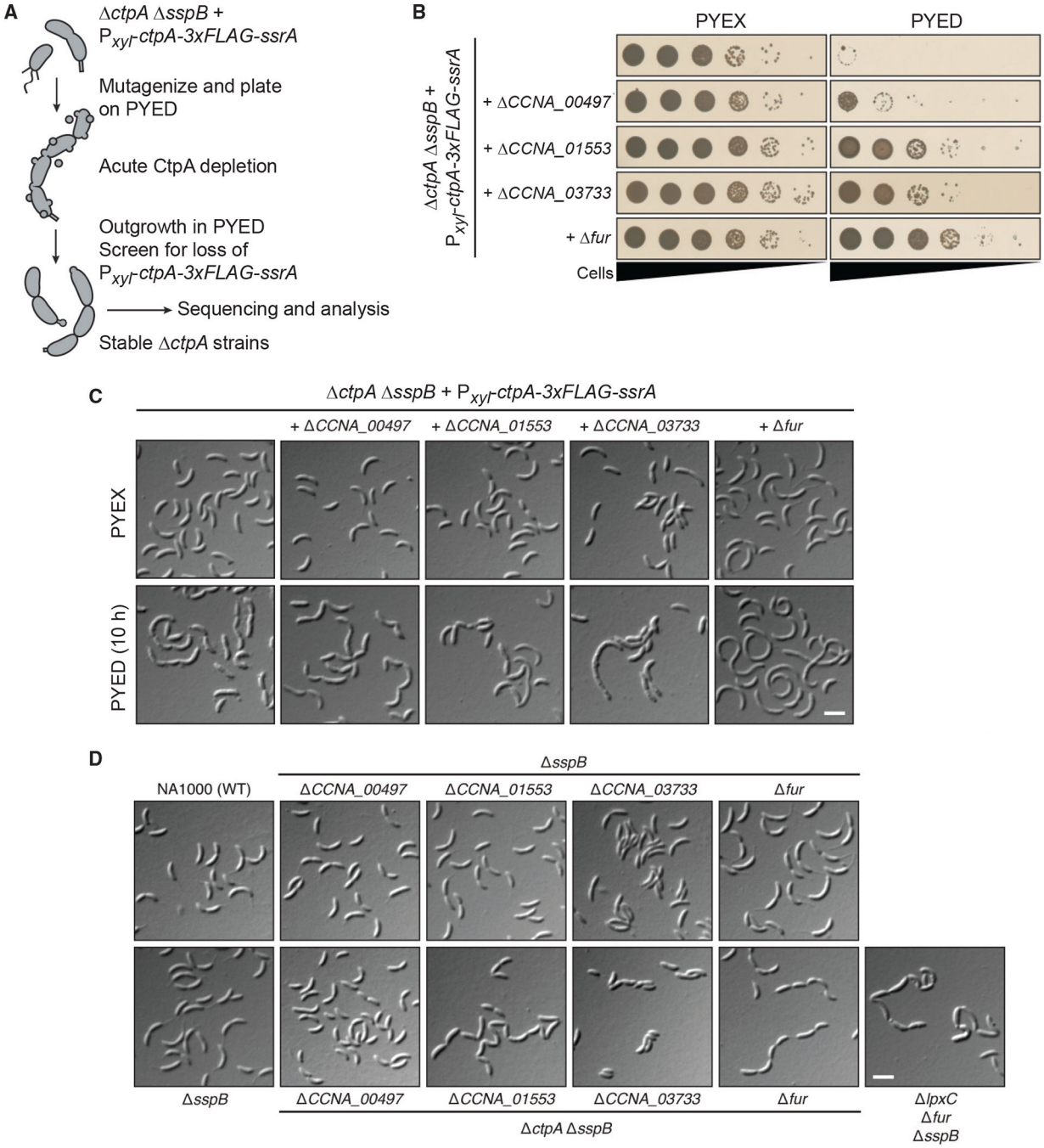


**Figure 1. Suppressor mutations affecting *fur* or O-antigen biosynthesis permit deletion of *ctpA***

(A) Strategy for isolating Δ*ctpA* suppressor mutants.

(B) Viability of suppressor strains during CtpA depletion on PYED.

(C) Differential interference contrast (DIC) images of strains grown under CtpA-expressing (PYEX) or non-expressing (PYED) conditions.

(D) DIC images of strains grown to exponential phase in PYE.

Scale bars, 3 μm. See also Figures S1 and S2 and Table S1.

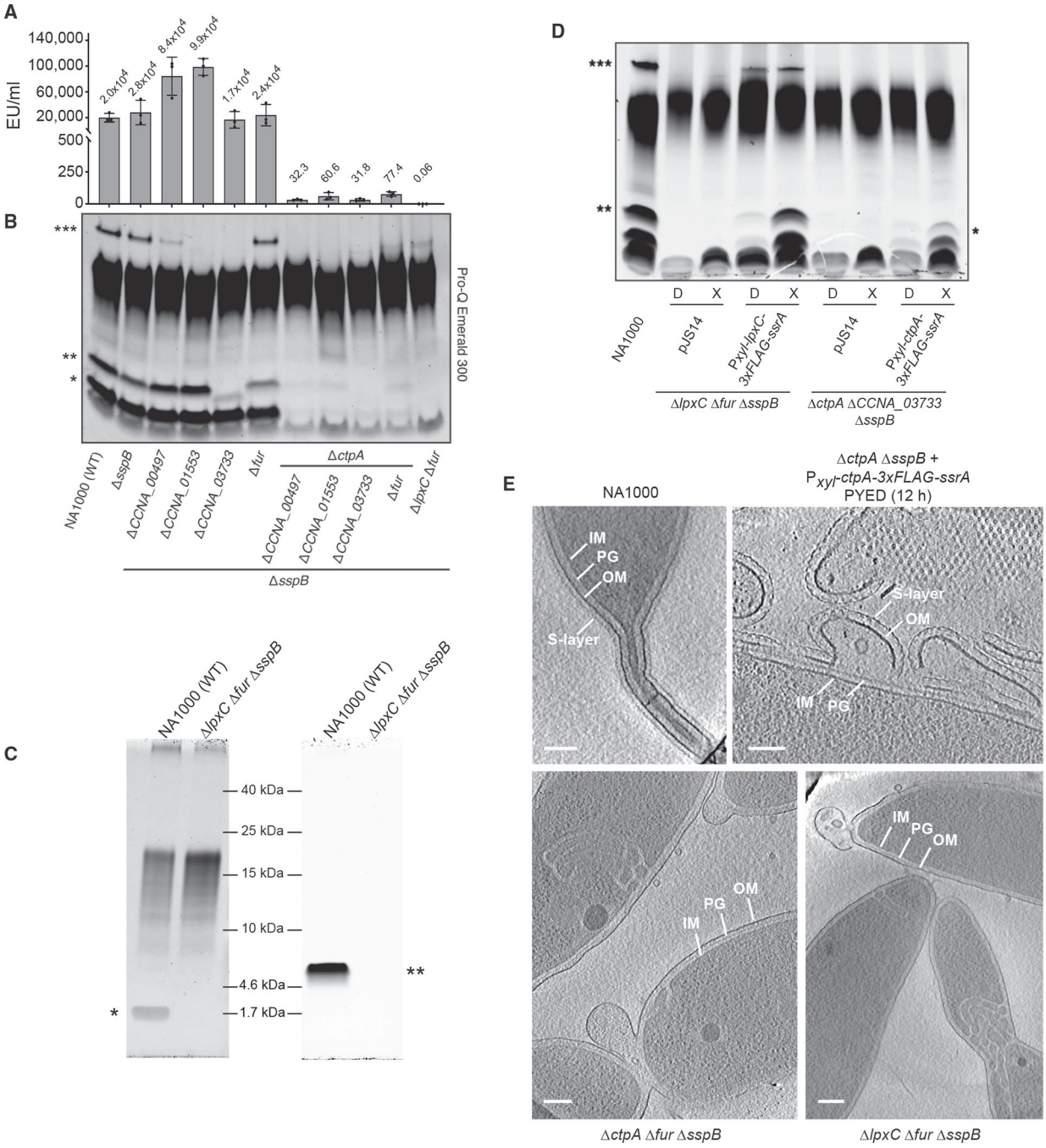


**Figure 2. Δ*ctpA* and Δ*lpxC* strains with suppressor mutations contain little or no lipid A**

(A) Endotoxin units (EU) per milliliter (mean ± SD) of whole cells of the strains indicated in (B). Dots represent individual data points, and mean values are displayed above bars.

(B) Hot aqueous phenol LPS extracts of the indicated strains. ***, S-LPS; **, putative full-length lipid A + core; *, putative lipid A.

(C) Lipid A (left) or rough LPS (right) extracted from the indicated strains. *, lipid A; **, rough LPS. A darker exposure of the same gel was used for lipid A lanes and a lighter

exposure for rough LPS lanes because the two sample types contained different amounts of material and were not normalized to each other.

(D) Proteinase K-treated lysates of the indicated strains maintained in PYED (D) or shifted into PYEX (X) for 6 h before harvesting. Samples were normalized by optical density at 660 nm ($OD_{660}$). NA1000 was grown in PYE. pJS14 denotes empty vector controls. Leaky expression of LpxC generates S-LPS (***) and lipid $A^+$ core (**) in PYED. Full-length S-LPS is not restored to *ctpA*, and its lipid $A^+$ core is reduced in size (*) because *CCNA_03733* is needed for mannose incorporation.

(E) Electron cryotomography images of the indicated strains, indicating the inner membrane (IM), peptidoglycan (PG), outer membrane (OM), and S layer. All strains were grown to exponential phase in PYE medium, except that CtpA was depleted from KR3906 during 12 h of growth in PYED prior to analysis.

Scale bars, 100 nm. See also Figure S3, Table S3, and Videos S1, S2, S3, and S4.

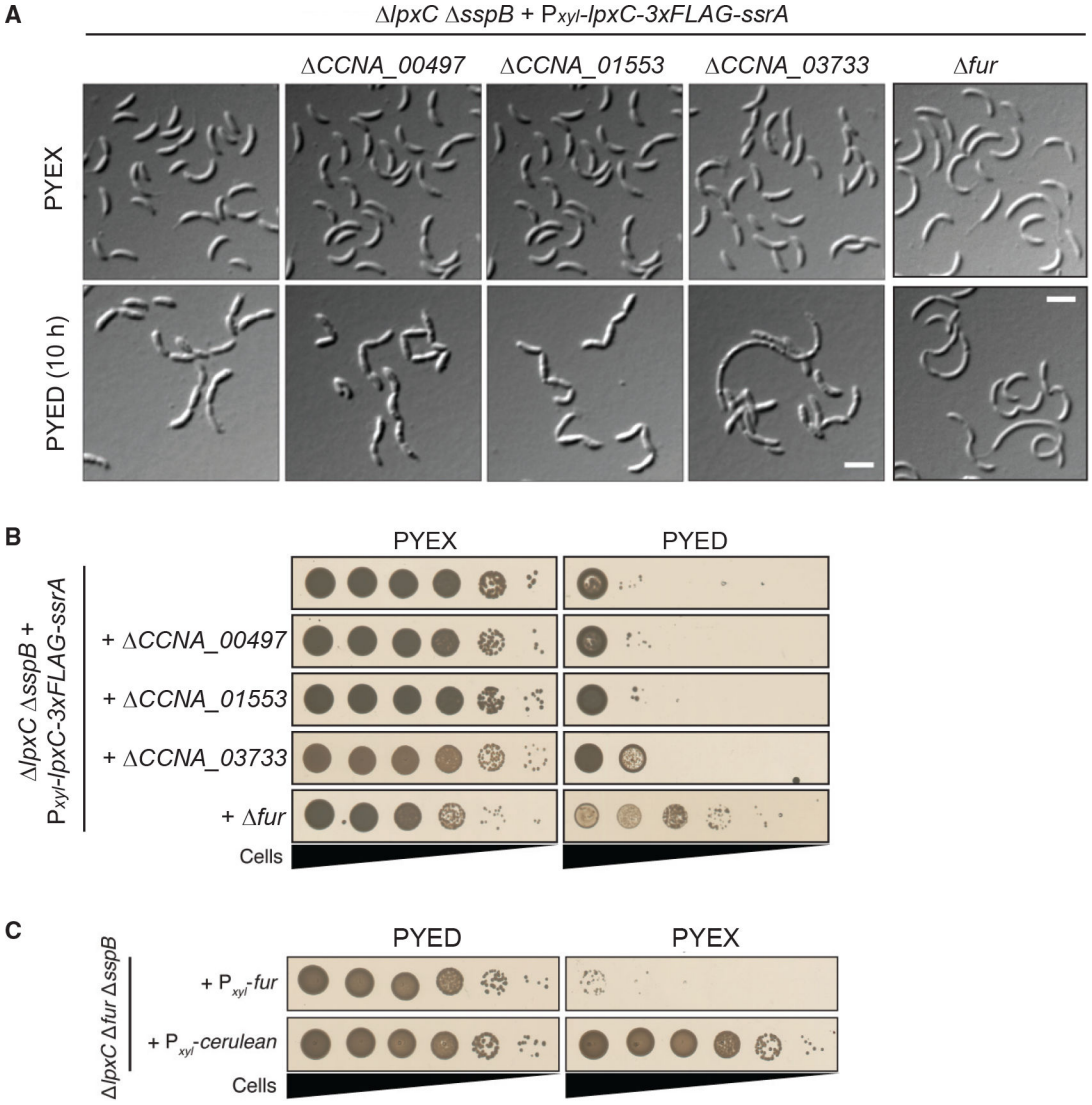


**Figure 3. Deletion of *fur* supports the viability of Δ*lpxC* cells**

(A) DIC images of the LpxC depletion strain alone or harboring the indicated mutations, grown in PYEX or PYED for 10 h. Scale bars, 3 μm.

(B) Viability of the LpxC depletion strain, alone or harboring the indicated mutations, plated on PYEX or PYED.

(C) Viability of Δ*lpxC* Δ*fur* Δ*sspB* cells harboring a Pxyl-*fur* or a Pxyl-*cerulean* expression vector. Plates included kanamycin to retain expression vectors.

See also Tables S2 and S5 and Figure S5.

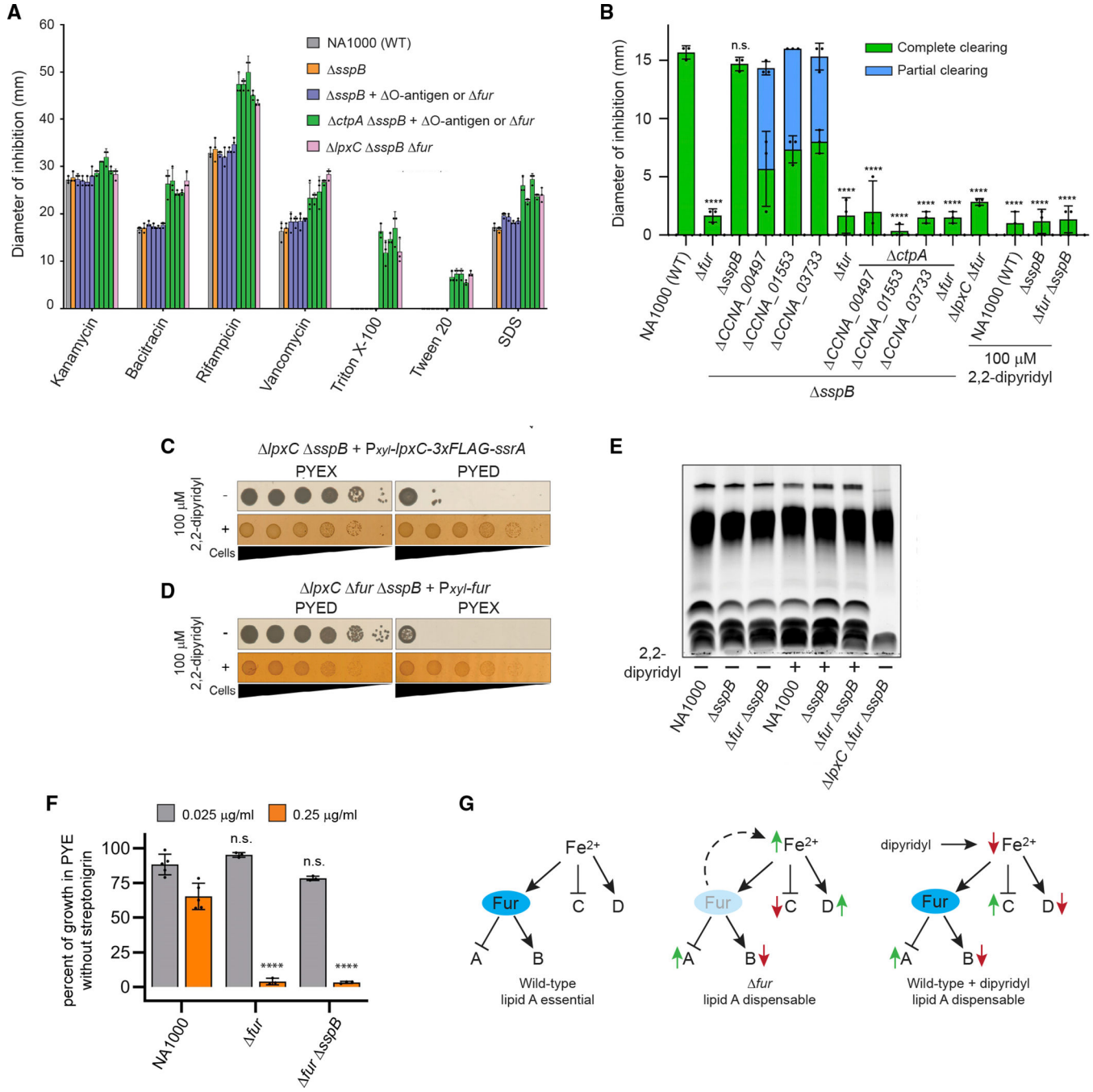


**Figure 4. Fur-regulated processes control the conditional essentiality of lipid A**

(A) Chemical sensitivity was measured by disc diffusion assay (mean ± SD). Dots indicate individual data points. Suppressor mutations present in strains represented by blue or green bars are, from left to right, *ΔCCNA_00497*, Δ*CCNA_01553*, Δ*CCNA_03733*, and Δ*fur*.

(B) CHIR-090 sensitivity measured by disc diffusion assay (mean ± SD). Partial clearing indicates the diameter of a ring of intermediate growth. Dots indicate individual measurements, and significance was tested by one-way ANOVA followed by Dunnett's

post-test comparison with NA1000. ****$p < 0.0001$; n.s., not significant. Strains exhibiting rings of partial growth were excluded from the analysis.

(C) Viability of the LpxC depletion strain under inducing (PYEX) or depleting (PYED) conditions in the presence or absence of 100 μM 2,2′-dipyridyl.

(D) Viability of Δ*lpxC* Δ*fur* Δ*sspB* cells harboring a Pxyl-*fur* plasmid, grown in noninducing (PYED) or inducing (PYEX) conditions in the presence or absence of 100 μM 2,2′-dipyridyl. Plates included kanamycin to retain the expression vector. Brightness was reduced and contrast increased to improve the clarity of colonies grown on 2,2′-dipyridyl.

(E) Proteinase K-treated lysates of the indicated strains grown overnight in the presence or absence of 100 μM 2,2′-dipyridyl. Samples were normalized by $OD_{660}$.

(F) Growth inhibition by SNG in liquid PYE cultures of the indicated strains (mean ± SD). Dots represent individual $OD_{660}$ ratios, and significance was tested by one-way ANOVA followed by Šídák's multiple comparisons test, where each strain was compared with NA1000 grown under the same condition. ****$p < 0.0001$; n.s., not significant.

(G) Changes in Fur-regulated gene expression correlate with the ability to survive in the absence of lipid A. Genes regulated by Fur in concert with iron (sets A and B) are modulated similarly by deletion of *fur* or by iron limitation, whereas genes regulated by iron alone (sets C and D) are modulated in opposite directions in these two conditions.

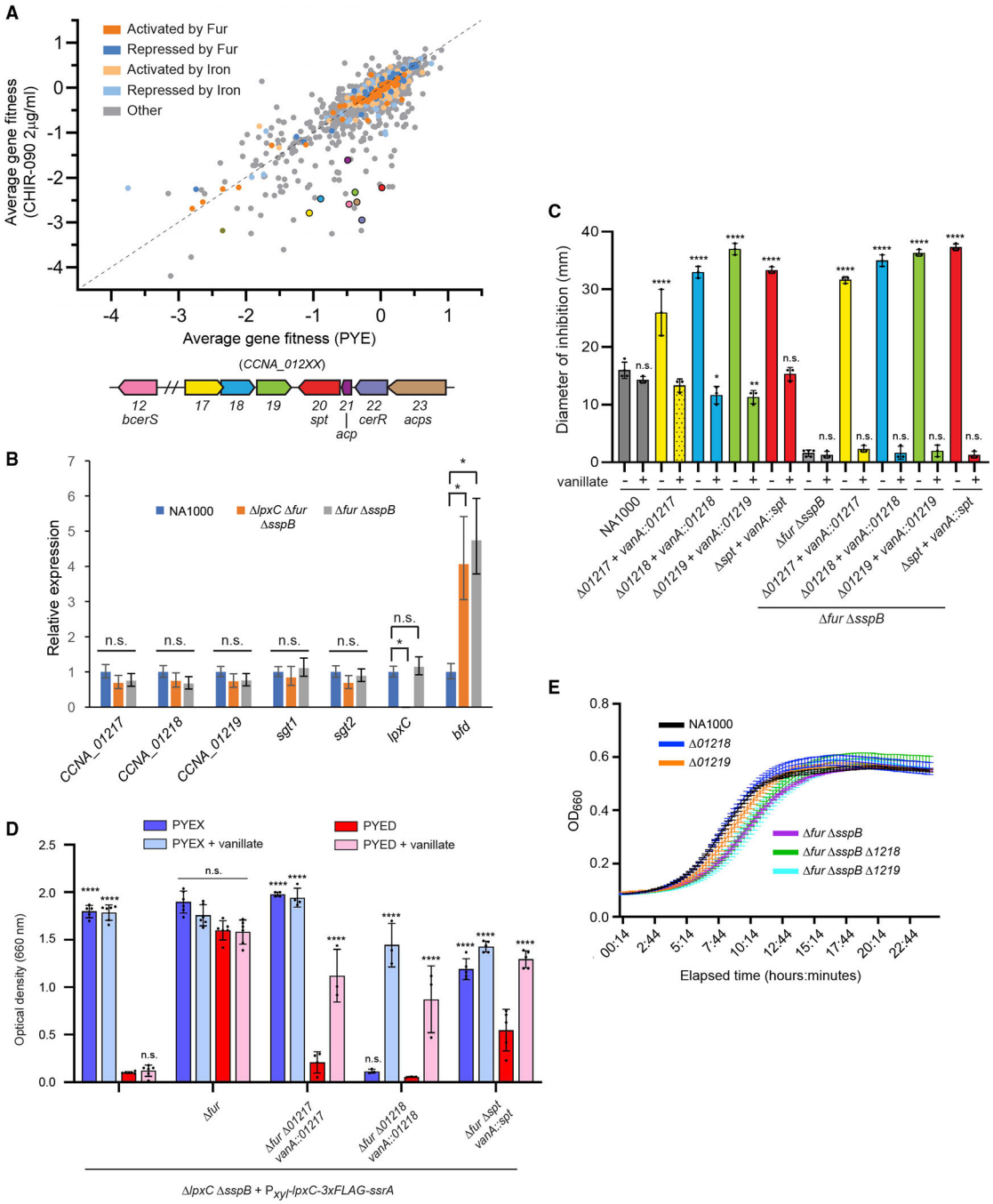


**Figure 5. RB-TnSeq identifies sphingolipid synthesis genes needed for fitness when LpxC is inhibited**

(A) Average gene fitness scores for three challenges of the NA1000 RB-TnSeq library with PYE or PYE + 2 µg/mL CHIR-090. Fitness scores are color-coded based on regulation of the corresponding genes. The average fitness scores of genes selected for analysis are indicated by colors matching the open reading frame diagram below. See also Table S4.

(B) Wild-type, Δ*fur* Δ*sspB*, and Δ*fur* Δ*lpxC* Δ*sspB* cells were grown to mid-log phase in PYE, and expression of the indicated genes was measured by qRT-PCR (N = 3 biological replicates, mean ± S.D). Gene expression was normalized to the wild-type sample for each

gene tested, and significance was tested by one-way ANOVA followed by Šídák's multiple comparisons test, where each strain was compared with the wild type.
(C) CHIR-090 sensitivity was measured by disc diffusion assay (mean ± SD). Where indicated, 0.5 mM vanillate was included in the medium. Dots represent individual measurements, and significance was tested by one-way ANOVA followed by Šídák's multiple comparisons test, where each condition was compared with NA1000 without vanillate or, for strains harboring Δ*fur* Δ*sspB*, with Δ*fur* Δ*sspB* without vanillate. The shaded bar indicates a ring of partial growth, and this condition was excluded from the analysis.
(D) Overnight growth of strains expressing (PYEX) or depleting (PYED) LpxC and expressing (vanillate) or not expressing the indicated genes (mean ± SD). Dots represent individual measurements, and significance was tested by one-way ANOVA followed by Šídák's multiple comparisons test, where each condition was compared with growth of the same strain in PYED.
(E) Growth curves of the indicated strains in PYE medium (mean ± SD).
The following symbols apply to all significance tests: ****$p < 0.0001$; ***$0.0001 < p < 0.001$; **$0.001 < p < 0.01$; *$0.01 < p < 0.05$; n.s., not significant $p > 0.05$.

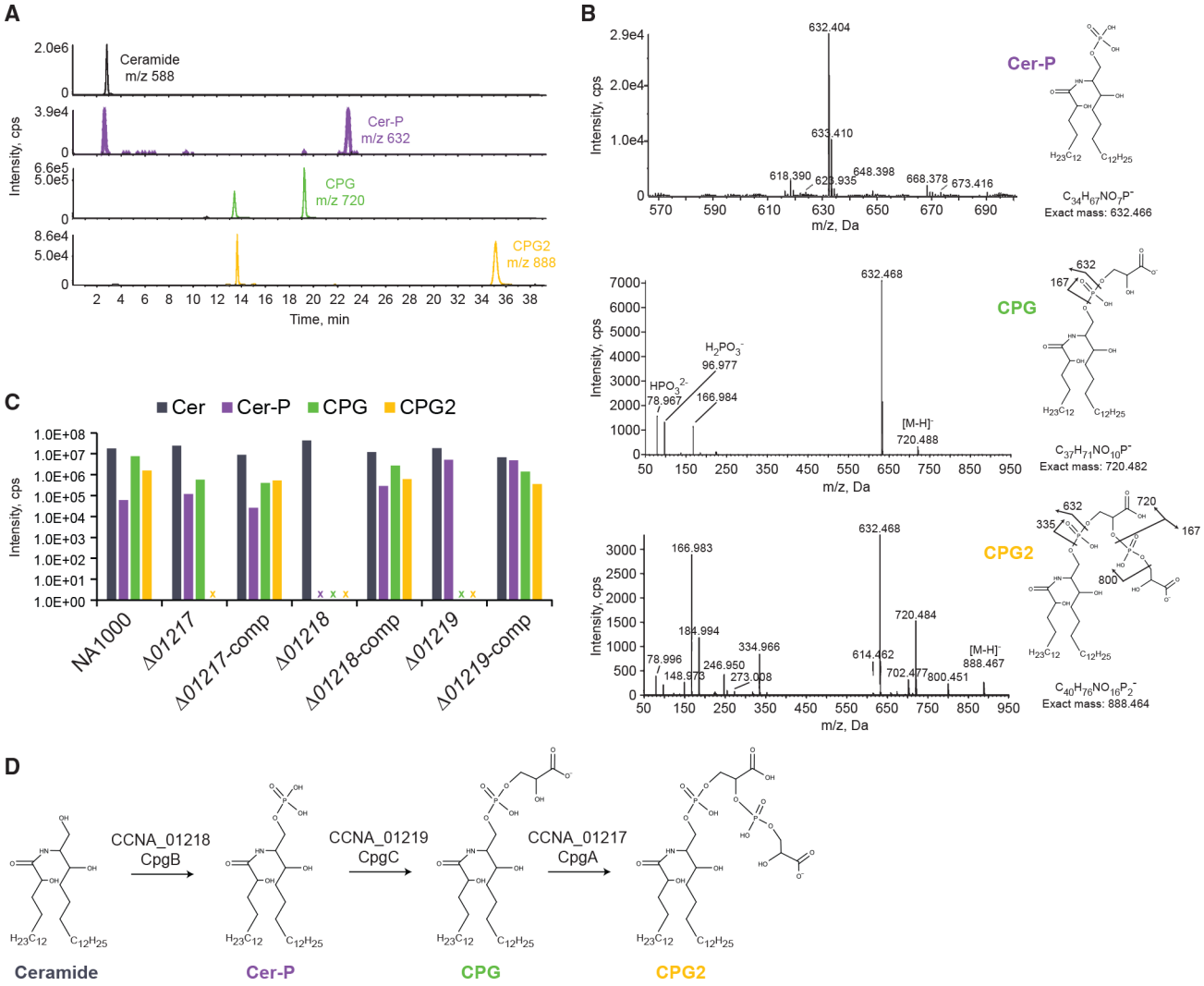


**Figure 6. *CCNA_01217-01219* convert neutral ceramide to CPG**

(A) Extracted ion chromatograms identified the indicated sphingolipid species in NA1000 lipid extracts.

(B) Structural determination of anionic sphingolipids was performed by MS/MS analysis.

(C) The presence of the indicated sphingolipids was assessed in each deletion mutant and its respective complemented strain. x, no lipid of that type was detected in the indicated strain. The presence of neutral ceramide served as an extraction control for each strain.

(D) Proposed mechanism for CPG2 synthesis.

See also Figure S4.

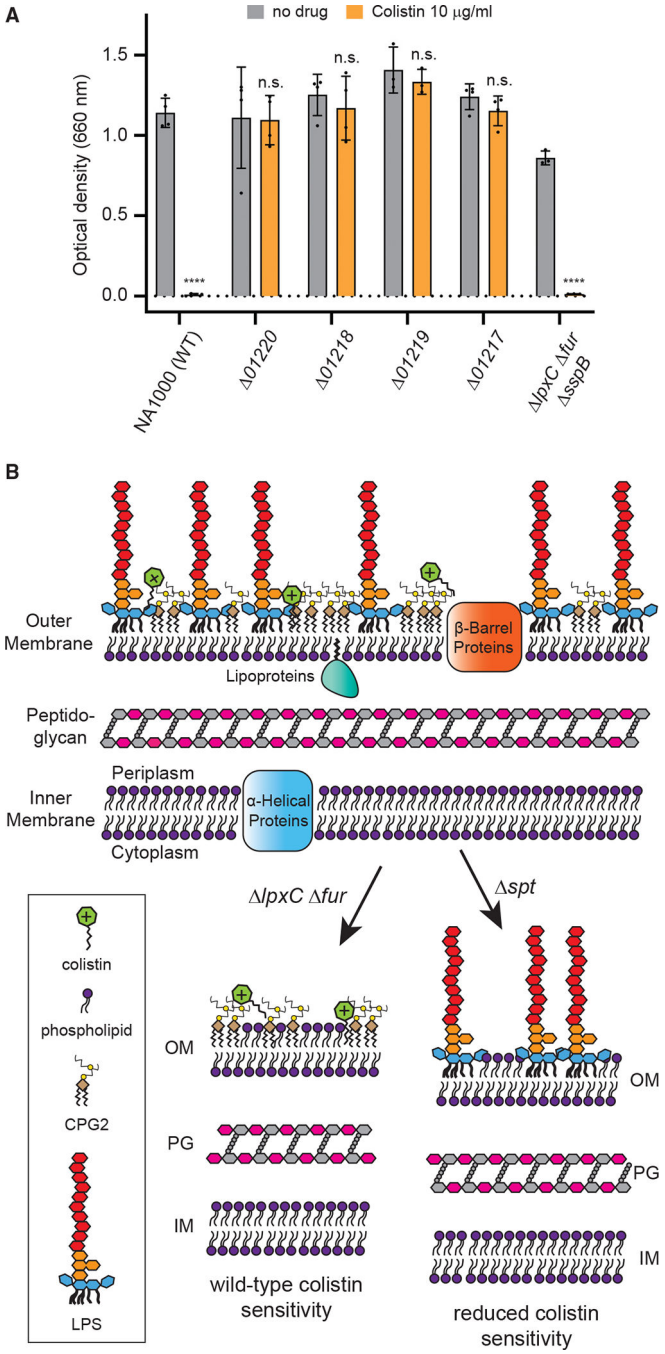


**Figure 7. CPG mediates susceptibility to colistin**

(A) Overnight growth of strains in the presence or absence of 10 μg/mL colistin (mean ± SD). Dots represent individual $OD_{660}$ measurements, and significance was tested by one-way ANOVA followed by Šídák's multiple comparisons test, where each strain treated with colistin was compared with the same strain without colistin. ****$p < 0.0001$; n.s., not significant.

(B) Model of the *Caulobacter* cell envelope containing LPS and CPG2, showing consequences for OM composition and colistin sensitivity when either lipid A (Δ*lpxC* Δ*fur*) or sphingolipids (Δ*spt*) are eliminated.

## KEY RESOURCES TABLE

| REAGENT or RESOURCE | SOURCE | IDENTIFIER |
|---|---|---|
| Antibodies | | |
| rabbit α-S-LPS (recognizes smooth LPS of *Caulobacter crescentus*) | John Smit, University of British Columbia; Walker et al., 1994 | N/A |
| Bacterial and virus strains | | |
| RB-TnSeq library constructed in *Caulobacter crescentus* NA1000 | Adam Deutschbauer, Lawrence Berkeley National Laboratory; Price et al., 2018 | N/A |
| *Caulobacter crescentus* NA1000 (CB15N) | Evinger and Agabian (1977); Lab collection | KR4000 |
| Δ*ctpA*::*tetAR* Δ*sspB*::*aadA* pAB6 | Shapland et al. (2011); Lab collection | KR3906 |
| Δ*lpxC*::*tetAR* Δ*sspB*::*aadA* pZIK133 | Lab collection | KR4007 |
| Δ*lpxC*::*tetAR* Δ*sspB*::*aadA* Δ*fur*::*hyg* pZIK133 | Lab collection | KR4091 |
| Δ*ctpA*::*tetAR* Δ*sspB*::*aadA* Δ*fur*::*hyg* | Lab collection | KR4102 |
| Δ*lpxC*::*tetAR* Δ*sspB*::*aadA* Δ*fur*::*hyg* | Lab collection | KR4103 |
| Δ*CCNA_01217 vanA*::*01217*::*FLAG* | Lab collection | KR4549 |
| Δ*CCNA_01218 vanA*::*01218*::*FLAG* | Lab collection | KR4505 |
| Δ*CCNA_01219 vanA*::*01219*::*FLAG* | Lab collection | KR4501 |
| Δ*CCNA_01220 vanA*::*01220*::*FLAG* | Lab collection | KR4530 |
| See Table S6 for a complete list of the bacterial strains constructed for this study | Lab collection | N/A |
| Chemicals, peptides, and recombinant proteins | | |
| streptonigrin | Sigma-Aldrich | Cat#S1014; CAS 3930-19-6 |
| Q5 High-Fidelity DNA Polymerase | New England Biolabs | Cat#M0491 |
| NEBuilder HiFi DNA Assembly Master Mix | New England Biolabs | Cat#E2621 |

| REAGENT or RESOURCE | SOURCE | IDENTIFIER |
|---|---|---|
| 2,2-dipyridyl | Thermo Scientific | Cat#AC117500100; CAS 366-18-7 |
| CHIR-090 | APExBIO | Cat#A3307; CAS 728865-23-4 |
| Bacto Peptone | Thermo Fisher | Cat# 211677; Lot# 9239004 |
| Agar Granulated Bacteriological Grade | Apex BioResearch Products | Cat#20-248; Lot#AB-2010160 |
| PowerUp SYBR Green Master Mix | Thermo Scientific | Cat#A25777 |
| High Capacity cDNA Reverse-Transcription Kit | Thermo Scientific | Cat#4368813 |
| DNeasy Blood & Tissue Kit | Qiagen | Cat#69504 |
| 16.5% Mini-PROTEAN Tris-Tricine gels | Bio-Rad | Cat#4563063 |
| RNeasy Kit | Qiagen | Cat#74004 |
| Critical commercial assays | | |
| Pro-Q Emerald 300 Lipopolysaccharide Gel Stain Kit | Thermo Fisher | Cat#P20495 |
| ToxinSensor Chromogenic LAL Endotoxin Assay | GenScript | Cat#L00350 |
| Deposited data | | |
| RB-TnSeq data | This paper | Fitness Browser https://fit.genomics.lbl.gov. *Caulobacter crescentus* NA1000 library grown in PYE medium: set8IT011, set8IT023, and set8IT035. *Caulobacter crescentus* NA1000 library grown in PYE medium with 2 μg/mL CHIR-090: set8IT012, set8IT024, and set8IT036. |
| Transcriptomic data for *Caulobacter crescentus* NA1000 wild-type, Δ*fur*, and wild-type treated with 2,2-dipyridyl | da Silva Neto et al., 2013 | N/A |
| Transcriptomic data for *Caulobacter crescentus* NA1000 wild-type, Δ*fur*, and wild-type treated with 2,2-dipyridyl | Leaden et al., 2018 | N/A |
| Genome sequences | This paper | Sequence Read Archive, https://www.ncbi.nlm.nih.gov/sra, BioProject ID PRJNA526705. Accession numbers for individual strains are listed in Table S6. |
| LC/MS analysis of sphingolipids | This paper; Mendeley Data | Mendeley Data: https://data.mendeley.com/datasets/hxxckxtb8p/2 |
| LC-MS/MS analysis of lipid A species | This paper; Mendeley Data | Mendeley Data: https://data.mendeley.com/datasets/y24rjwkb48/1 |
| Experimental models: Organisms/strains | | |
| *Caulobacter crescentus* NA1000 (CB15N) | Evinger and Agabian (1977); Lab collection | KR4000 |
| Oligonucleotides | | |

| REAGENT or RESOURCE | SOURCE | IDENTIFIER |
|---|---|---|
| See Table S8 for a complete list of oligonucleotides used in this study | Integrated DNA Technologies (IDT) | https://www.idtdna.com/pages |
| Recombinant DNA | | |
| pZIK133: pJS14-*$P_{xylX}$::lpxC::3xFLAG::ssrA* | Lab collection | KR3969 |
| pAB6: pJS14-*$P_{xylX}$::ctpA::3xFLAG::ssrA* | Lab collection | KR2419 |
| See Table S7 for a complete list of plasmids used in this study | Lab collection | N/A |
| Software and algorithms | | |
| Bowtie2 | Langmead and Salzberg (2012) | http://bowtie-bio.sourceforge.net/bowtie2/index.shtml |
| FreeBayes | Garrison and Marth (2012) | https://github.com/freebayes/freebayes |
| iVision-Mac | BioVision Technologies | https://www.biovis.com/bodies/ivision.html |
| ImageJ | Rasband, W.S., ImageJ, U. S. National Institutes of Health, Bethesda, Maryland, USA, https://imagej.nih.gov/ij/, 1997–2018 | https://ImageJ.nih.gov/ij/download.html |
| MotionCor2 | Zheng et al., 2017 | https://emcore.ucsf.edu/ucsf-software |
| AMIRA | Thermo Fisher | https://www.thermofisher.com/us/en/home/electron-microscopy/products/software-em-3d-vis/amira-software.html |
| Analyst TF1.5 | Applied Biosystems | https://sciex.com/form-pages/sw-downloads-form?d=Analyst-1.5.1-WebRelease.zip&asset=software&softwareProduct=Analyst%C2%AE%201.5.1%20Software |
| Galaxy | Afgan et al., 2016 | https://usegalaxy.org/ |
| Cutadapt | Martin (2011) | https://cutadapt.readthedocs.io/en/stable/ |
| GraphPad Prism 9.3.1 | GraphPad Software, LLC | https://www.graphpad.com/ |
| IMOD | Kremer et al., 1996 | https://bio3d.colorado.edu/imod/ |
| serialEM | Mastonarde, 2005 | https://bio3d.colorado.edu/SerialEM/ |